HEAT TRANSFER FROM ELECTRICALLY HEATED THIN METAL FILMS IN VACUO

A THESIS

Presented to

The Faculty of the Graduate Division

by

Robert Roy Swank, Jr.

In Partial Fulfillment

of the Requirements for the Degree

Doctor of Philosophy in the School of Chemical Engineering

Georgia Institute of Technology

May, 1968

In presenting the dissertation as a partial fulfillment of the requirements for an advanced degree from the Georgia Institute of Technology, I agree that the Library of the Institute shall make it available for inspection and circulation in accordance with its regulations governing materials of this type. I agree that permission to copy from, or to publish from, this dissertation may be granted by the professor under whose direction it was written, or, in his absence, by the Dean of the Graduate Division when such copying or publication is solely for scholarly purposes and does not involve potential financial gain. It is understood that any copying from, or publication of, this dissertation which involves potential financial gain will not be allowed without written permission.

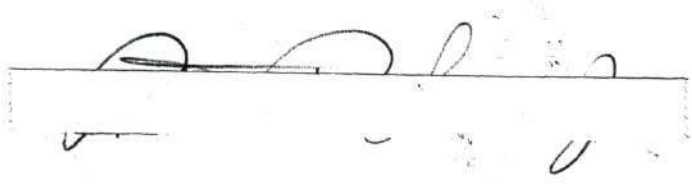

3/17/65
b

HEAT TRANSFER FROM ELECTRICALLY HEATED THIN METAL FILMS IN VACUO

Approved:

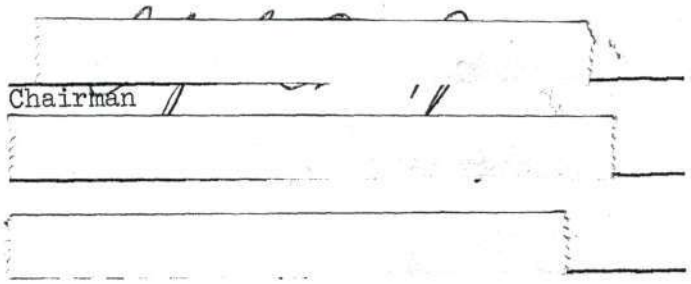

Chairman

Date approved by Chairman: May 27, 1968

ACKNOWLEDGMENTS

The author wishes to express his most sincere gratitude and appreciation to Dr. Julian D. Fleming, Jr. and Dr. Clyde Orr, Jr. who served so capably as thesis advisors for this work--to Dr. Fleming for his inspiration and guidance in establishing the problem and directing its progress, and to Dr. Orr who so graciously accepted the task of supervising its completion following the departure of Dr. Fleming from the faculty.

The author is also indebted to Messrs. Jesse D. Walton and Nick E. Poulos who made experimental facilities available, to Dr. Steve H. Bomar, Jr. and Mr. James W. Johnson who provided technical assistance, to Dr. Charles W. Gorton and Dr. Frederick Bellinger who assisted in the thesis preparation, and to Dr. Homer V. Grubb for his kind cooperation and patience.

The author should also like to express his eternal gratitude to his parents for their personal sacrifices and wise counciling which provided both the opportunity and climate for this educational experience, and to his wife for her love, patience, faith, and understanding without which the entire program would have been impossible.

In addition to these persons, the author must also recognize the generous financial support of the Texaco Company, the National Science Foundation, and the United States Public Health Service, Division of Air Pollution, which made the doctoral program a financial reality.

TABLE OF CONTENTS

Page

ACKNOWLEDGMENTS ii

LIST OF TABLES v

LIST OF ILLUSTRATIONS viii

SUMMARY xiii

Chapter

I. INTRODUCTION 1

Historical Background
Purpose of This Research
Related Literature

II. EXPERIMENTAL INSTRUMENTATION AND EQUIPMENT 7

General
Data Recording System
Film Test Power Supply
Vacuum Test/Plating System
Temperature-Resistance Film Calibration System

III. EXPERIMENTAL PROCEDURES 35

Thin Metal Film Production
Thermometric Calibration of the Test Film
Data Recording System Calibration
Vacuum Film Tests
Conversion of Photographic Data to Thermal Parameters

IV. THE EFFECT OF THICKNESS, TEMPERATURE, AND TEMPERATURE CYCLING ON THIN METAL FILM ELECTRICAL RESISTANCE 53

Background
Thin Film Resistance Stability Under External Cyclic Heating in Vacuo
Experimental Procedure
Discussion of Stability Results
Film Resistance and Resistivity Dependence on Film Thickness

TABLE OF CONTENTS (Continued)

Page

Chapter

IV. (Continued)

Film Temperature Coefficient of Resistance Dependence on Film Thickness

V. FILM UNIFORMITY AND THICKNESS DISTRIBUTION 74

Background
General
Sample Preparation
X-Ray Fluorescence Analysis
Weight-Fluorescence Correlation and Thickness Distribution
Theoretical Prediction of Thickness Distribution
Discussion of Film Thickness Uniformity Results

VI. RESULTS AND DISCUSSION OF THE VACUUM THERMAL TESTS 100

Thin Film Thermal Test Data
Substrate Conduction Analysis
Film Surface Temperature Distribution Analysis
Formulation of a Failure Mechanism for Thin Metal Films When Subjected to Rapid Transient Ohmic Heating
Comparison of Vacuum Thin Film Tests with Exploding Foil and Wire Experiments
Discussion of Experimental Errors

VII. CONCLUSIONS AND RECOMMENDATIONS 193

APPENDICES

I. FILM THICKNESS DISTRIBUTION DATA 200

II. HEAT TRANSFER DATA FOR EXPERIMENTAL FILMS 213

III. PLOTTED CALIBRATION AND HEAT TRANSFER DATA FOR EXPERIMENTAL FILMS 270

IV. SUBSTRATE CONDUCTION HEAT FLUX MODEL DERIVATION 292

BIBLIOGRAPHY 310

VITA 313

LIST OF TABLES

Table		Page
1.	Calibration Furnace Electrical Lead and Connection Resistance Versus Calibration Temperature	45
2.	Stability Test Film Characteristics Summary	56
3.	Film Failure Condition Summary	109
4.	"Log-Linear Phase" Test Film Parameters	122
5.	"Notch" Parameters and Dimensions for Film Surface Temperature Distribution Analysis	132
6.	Film Metal Average Values of the Modified Film Temperature Coefficient of Resistance β'	141
7.	Model Results Summary at Experimental Film Breakaway Point	165
8.	Model Results Summary at Experimental Film Failure Point	169
9.	Weight-Fluorescence Correlation Data for Copper Uniformity Film No. 1	201
10.	Weight-Fluorescence Correlation Data for Copper Uniformity Film No. 2	202
11.	Weight-Fluorescence Correlation Data for Copper Uniformity Film No. 3	203
12.	Weight-Fluorescence Correlation Data for Copper Uniformity Film No. 4	204
13.	Weight-Fluorescence Correlation Data for Nickel Uniformity Film No. 1	205
14.	Weight-Fluorescence Correlation Data for Nickel Uniformity Film No. 2	206
15.	Weight-Fluorescence Correlation Data for Nickel Uniformity Film No. 3	207
16.	Weight-Fluorescence Correlation Data for Nickel Uniformity Film No. 4	208

LIST OF TABLES (Continued)

Tables		Page
17.	Weight-Fluorescence Correlation Data for Nickel Uniformity Film No. 5	209
18.	Film Thickness Distribution Summary For Copper Films	210
19.	Film Thickness Distribution Summary For Nickel Films	211
20.	Theoretical Thickness Distribution Dimensionless Ratios	212
21.	Data for Copper Film No. 4, Series 1	214
22.	Data for Copper Film No. 5, Series 1	217
23.	Data for Copper Film No. 6, Series 1	219
24.	Data for Copper Film No. 1, Series 2	221
25.	Data for Copper Film No. 2, Series 2	224
26.	Data for Copper Film No. 3, Series 2	227
27.	Data for Copper Film No. 5, Series 2	230
28.	Data for Copper Film No. 6, Series 2	233
29.	Data for Nickel Film No. 7	236
30.	Data for Nickel Film No. 8	238
31.	Data for Nickel Film No. 9	241
32.	Data for Nickel Film No. 10	244
33.	Data for Nickel Film No. 15	247
34.	Data for Aluminum Film No. 2	250
35.	Data for Aluminum Film No. 3	253
36.	Data for Aluminum Film No. 4	255
37.	Data for Aluminum Film No. 5	258

LIST OF TABLES (Continued)

Table		Page
38.	Data for Aluminum Film No. 6	261
39.	Data for Aluminum Film No. 7	264
40.	Data for Aluminum Film No. 8	267
41.	Values of the Error Function, Its Derivatives, and Its Repeated Integrals	307
42.	Substrate Thermal Property Data Summary	308

LIST OF ILLUSTRATIONS

Figure		Page
1.	FM Magnetic Tape Recording System and Dual Beam Oscilloscope	9
2.	Schematic Diagram of Data Recording and Storage System	10
3.	Ideal 3-Phase Bridge Rectifier Output and Typical Film Voltage and Current Trace	15
4.	Schematic Diagram of DC Power Supply	18
5.	Panoramic View of Set-Up Film Test Vacuum Chamber, Power Supply, and Instrument Work Bench	19
6.	Vacuum Chamber Set-Up for Film Plating Operation with Detail of Substrate-Filament Geometry and Instrumentation	23
7.	Film Holder Assembly in Test Chamber, Plus Detail Drawing of Film-End Block Assembly Connection	25
8.	Temperature-Resistance Film Calibration System with Partial Top View of Vacuum Furnace	31
9.	Data Recording System Calibration Wiring Diagram	46
10.	Cyclic Resistance Stability for Copper Films	57
11.	Cyclic Resistance Stability for Nickel Films	58
12.	Cyclic Resistance Stability for Aluminum Films	59
13.	Post-Test Appearance of Cyclic High Temperature Stability Films	60
14.	Copper Film Room Temperature Resistance and Resistivity Thickness Dependence	66
15.	Nickel Film Room Temperature Resistance and Resistivity Thickness Dependence	67
16.	Aluminum Film Room Temperature Resistance and Resistivity Thickness Dependence	68

LIST OF ILLUSTRATIONS (Continued)

Figure		Page
17.	Calibration Average Temperature Coefficient of Resistance Versus Average Thickness for Copper, Nickel, and Aluminum Films	73
18.	Film Thickness Investigation Substrate Division, Marking, and X-Ray Fluorescence Exposure Pattern	77
19.	Weight-X-Ray Fluorescence Film Thickness Calibration Curve for Copper	82
20.	Weight-X-Ray Fluorescence Film Thickness Calibration Curve for Nickel	83
21.	Thickness Distribution Profiles for Copper Uniformity Films 1 and 2	84
22.	Thickness Distribution Profiles for Copper Uniformity Films 3 and 4	85
23.	Thickness Distribution Profiles for Nickel Uniformity Films 1 and 2	86
24.	Thickness Distribution Profiles for Nickel Uniformity Films 3 and 4	87
25.	Source-Substrate Geometry and Nomenclature for Theoretical Thickness Distribution Calculation	90
26.	Theoretical Thickness Distribution Profiles for "Ideal" and "Typical" Plating Conditions	94
27.	Heat Flux Curves for Short-Time Copper Tests	102
28.	Heat Flux Curves for Mid-Time Copper Tests	103
29.	Heat Flux Curves for Long-Time Copper Tests	104
30.	Heat Flux Curves for Short-Time Nickel Tests	105
31.	Heat Flux Curves for Long-Time Nickel Tests	106
32.	Heat Flux Curves for Short-Time Aluminum Tests	107
33.	Heat Flux Curves for Long-Time and Incomplete Aluminum Tests	108

LIST OF ILLUSTRATIONS (Continued)

Figure		Page
34.	Post-Test Appearance of Figure 27. Copper Films	111
35.	Post-Test Appearance of Figure 28. Copper Films	112
36.	Post-Test Appearance of Figure 29. Copper Films	113
37.	Post-Test Appearance of Figure 30. Nickel Films	115
38.	Post-Test Appearance of Figure 31. Nickel Films	116
39.	Post-Test Appearance of Figure 32. Aluminum Films	117
40.	Post-Test Appearance of Figure 33. Aluminum Films	118
41.	Time Exposure Photographs of Copper Film No. 3, Series 2 Failure Event	119
42.	Copper Film No. 6, Series 2 Failure Event and Blow-Up of the Positive Electrical Contact Zone of Post-Tested Nickel Film No. 15	120
43.	Assumed Film Geometry and Variable Definition for Film Surface Temperature Distribution Modeling	129
44.	Calculated "Notch" and Thick Zone Temperatures Versus Film Average Temperature for Each Copper Film Quality Based Upon the Volumetric Heat Generation Assumption	138
45.	Calculated "Notch" and Thick Zone Temperatures Versus Film Average Temperature for Each Nickel Film Quality Based Upon the Volumetric Heat Generation Assumption	139
46.	Calculated "Notch" and Thick Zone Temperatures Versus Film Average Temperature for Each Aluminum Film Quality Based Upon the Volumetric Heat Generation Assumption	140
47.	Calculated "Notch" and Thick Zone Temperatures Versus Film Average Temperature for Each Copper Film Quality Based Upon the Substrate Conduction Heat Flux Assumption . .	144
48.	Calculated "Notch" and Thick Zone Temperatures Versus Film Average Temperature for Each Nickel Film Quality Based Upon the Substrate Conduction Heat Flux Assumption . .	145

LIST OF ILLUSTRATIONS (Continued)

Figure		Page
49.	Calculated "Notch" and Thick Zone Temperatures Versus Film Average Temperature for Each Aluminum Film Quality Based Upon the Substrate Conduction Heat Flux Assumption . .	146
50.	Film to End Plate Radiation Shape Factor Geometry and Dimensions	151
51.	Thermometric Calibration, Heat Flux, and Film Temperature Data for Copper Film No. 4, Series 1	271
52.	Thermometric Calibration, Heat Flux, and Film Temperature Data for Copper Film No. 5, Series 1	272
53.	Thermometric Calibration, Heat Flux, and Film Temperature Data for Copper Film No. 6, Series 1	273
54.	Thermometric Calibration, Heat Flux, and Film Temperature Data for Copper Film No. 1, Series 2	274
55.	Thermometric Calibration, Heat Flux, and Film Temperature Data for Copper Film No. 2, Series 2	275
56.	Thermometric Calibration, Heat Flux, and Film Temperature Data for Copper Film No. 3, Series 2	276
57.	Thermometric Calibration, Heat Flux, and Film Temperature Data for Copper Film No. 5, Series 2	277
58.	Thermometric Calibration, Heat Flux, and Film Temperature Data for Copper Film No. 6, Series 2	278
59.	Thermometric Calibration, Heat Flux, and Film Temperature Data for Nickel Film No. 7	279
60.	Thermometric Calibration, Heat Flux, and Film Temperature Data for Nickel Film No. 8	280
61.	Thermometric Calibration, Heat Flux, and Film Temperature Data for Nickel Film No. 9	281
62.	Thermometric Calibration, Heat Flux, and Film Temperature Data for Nickel Film No. 10	282
63.	Thermometric Calibration, Heat Flux, and Film Temperature Data for Nickel Film No. 15	283

LIST OF ILLUSTRATIONS (Continued)

Figure — Page

64. Thermometric Calibration, Heat Flux, and Film Temperature Data for Aluminum Film No. 2, Test 1 284

65. Thermometric Calibration, Heat Flux, and Film Temperature Data for Aluminum Film No. 2, Test 2 285

66. Thermometric Calibration, Heat Flux, and Film Temperature Data for Aluminum Film No. 3 286

67. Thermometric Calibration, Heat Flux, and Film Temperature Data for Aluminum Film No. 4 287

68. Thermometric Calibration, Heat Flux, and Film Temperature Data for Aluminum Film No. 5 288

69. Thermometric Calibration, Heat Flux, and Film Temperature Data for Aluminum Film No. 6 289

70. Thermometric Calibration, Heat Flux, and Film Temperature Data for Aluminum Film No. 7 290

71. Thermometric Calibration, Heat Flux, and Film Temperature Data for Aluminum Film No. 8 291

72. Substrate Geometry and Coordinates for Substrate Conduction Heat Flux Model Derivation 294

SUMMARY

This thesis presents an investigation of the intrinsic properties, characteristics, operating condition limitations, and failure mechanisms exhibited by thin metal films whenever they are used as simultaneous resistance thermometers and heating elements in rapid transient, high flux studies. The investigation was conducted with vacuum vapor deposited films of copper, nickel, and aluminum on heated, polished fused quartz substrates. These three metals were chosen because they are similar metallurgically, being face centered cubic, are easy to fabricate, and possess as a set a considerable range of thermal and electrical conductivities, melting temperatures, and other physical properties. In order to evaluate only the intrinsic properties of these films, the available thermal transport modes were reduced to those always available, namely, conduction to the substrate, end loss, and radiation, by transiently heating them under a nominal vacuum of 10^{-5} mm of Hg. Suitable high speed instrumentation techniques were employed to monitor instantaneous film voltage and current throughout each test. Instantaneous film average temperatures were obtained from the film resistance data, since each film was calibrated as a resistance thermometer prior to its transient heating.

The advent of modern technology, with its increasing use of processes requiring very large heat fluxes and high operating temperatures, has created a need for developing flexible, inexpensive laboratory techniques for investigating these conditions. Other researchers have proposed the use of thin metal films, possessing both large surface area and signifi-

cant electrical resistance, as low current, high voltage resistance heating elements and thermometers for such laboratory application. A few researchers have already attempted the use of similar thin metal films as simultaneous resistance heaters and thermometers in transient, high flux studies involving swirling and boiling fluids with limited success and considerable difficulty in the area of data interpretation.

The purpose of this study was to reveal those intrinsic properties of thin metal films that may have played a role in the difficulties encountered in previous applications and to aid thereby in the improved planning and fruitful use of thin films in future studies. The test films used in this study were three or four inches long by one inch wide, with thicknesses ranging from 2000 to 6000 Å for copper, 1000 to 3500 Å for nickel, and 600 to 4600 Å for aluminum. The films were heated with continuously variable direct current, utilizing a specially designed copper knife blade electrical lead system, with test durations ranging from 0.5 to 15 seconds. The film voltage and current were recorded on a high-speed tape recorder and played back at 1/200th of the recording speed through a dual beam oscilloscope. The screen was photographed, and the electrical parameters were determined from enlargements of the oscilloscope screen negatives. Instantaneous values of the power dissipation, film average heat flux, and film average temperature were then calculated. Attempts were also made to monitor both the substrate and vacuum ambient temperature immediately above the film surface during the course of several tests.

As a data base point of departure, film resistance stability and overall behavior for each test metal was examined by subjecting a typical film of each metal to extensive externally heated, cyclic vacuum thermometric

calibration in which the temperatures were made to exceed the maximum film average temperature exhibited by that metal during the transient tests. The results of these stability examinations are included in this work.

A mathematical model was developed to correlate and crosscheck the measured film average temperature-time data with the measured film average substrate heat flux-time data for each test film. In addition, an X-ray fluorescence thickness distribution analysis was conducted, the results of which were quantified and used as input for three "notch" models formulated to estimate the film surface temperature distribution corresponding to any measured film average value. The "notch" model results aided in the interpretation of various experimental observations and served to hypothesize a film failure mechanism.

Maximum power levels observed in the transient tests of this study prior to failure were 1260 watts for copper films, 1780 watts for nickel films, and 390 watts for aluminum films. The corresponding film average temperatures and substrate heat fluxes were 890°F and 225,000 Btu/hr-ft^2 for copper, 790°F and 312,000 Btu/hr-ft^2 for nickel, and 400°F and 74,000 Btu/hr-ft^2 for aluminum. Higher apparent film average temperatures were observed at the moment of failure for these films, but at lower power levels. However, because of severe temperature anisotropy the average value at that point had little significance. The maximum observed film average temperature in this study having any significance was that of a very slowly heated four-inch long copper film that reached approximately 1200°F prior to failure. The corresponding power level was 630 watts, or an average flux of 78,000 Btu/hr-ft^2. These tests were conducted with maximum dc currents ranging from 20 to 60 amperes and maximum applied dc

voltages ranging from 20 to 60 volts.

In almost every test, even in those films of excellent uniformity, failure was caused by apparent tensile rupture at or near heat sinks or stress concentrating factors such as the electrical lead contact blades or known surface flaws such as scratches. Unexpected visual phenomena such as striation formation, running surface arcs, and avalanching were observed at rupture suggestive of exploding wire and foil behavior. Large temperature anisotropy was a problem even with good quality films of high conductivity in low-heating rate tests. The films were capable of breakaway behavior, i.e., once heated to some level they were capable of undergoing rupture at constant voltage. Reasons are given to show that the breakaway behavior would occur if any part of the film was heated above the recrystallization temperature while at the same time another part was held significantly below that value.

In short, the study revealed that from a manipulative point of view the use of high-speed instrumentation makes the use of thin films as simultaneous resistance heaters and thermometers in high flux, transient situations feasible. However, the practical use of the thin films depends strongly on the intrinsic limitations of the film metal chosen. Particularly, high recrystallization temperatures are required for high temperature application in combination with extreme uniformity and high thermal conductivity if film average quantities are to have any meaning. Better electrical lead design to eliminate film-substrate weakness, stress concentrating factors, and the heat sink effect is mandatory if operation above the metal recrystallization temperature is to be attempted, regardless of film properties. The use of a substrate with a thermal expansion

coefficient more nearly equal to that of the film metal in combination with a film which has been annealed prior to calibration is suggested to reduce the intrinsic film tensile stress levels. Such action should permit the extension of useful thin film temperatures above the recrystallization temperature for present electrical lead designs. As a result of this work, it is concluded that the intrinsic limitations of thin films employed as simultaneous resistance heaters and thermometers, particularly the tendency and capability for thermal independence of various thickness zones and the breakaway phenomena, played a significant role in the behavior and failure processes encountered by previous researchers so employing thin films, but who ascribed their observed film behavior, for the most part, to other mechanisms.

CHAPTER I

INTRODUCTION

The advent of nuclear reactors and space age technology has greatly increased the interest in high temperature, high heat flux, transient thermal transport processes and mechanisms. The need for extensive laboratory scale research of such processes has severely taxed conventional electrical power experimental techniques and created an interest in the possible use of thin metal films deposited on non-conducting substrates as simultaneous resistance thermometers and heating elements for such laboratory use.

This investigation records the attempt to ascertain and reveal those properties and characteristics intrinsic to the thin films themselves that might limit or have a significant effect on their proposed use. In order to conduct this investigation, the thin film performance of three metallurgically similar, face centered cubic, but otherwise different metals, copper, nickel, and aluminum, were analyzed and compared. The tests were conducted under a high vacuum at heating rates commensurate with those required for other proposed thermal studies. The vacuum test environment was chosen to reduce the available thermal transport modes to those intrinsic to the thin film-substrate system and to provide a chemically inert environment at the expected high temperatures prior to failure. In addition, the restriction of the available thermal transport modes permits comparison between mathematical modeling results and experimental measure-

ments. The film behavior in each test was continuously monitored up to its failure by means of suitable high-speed instrumentation.

Historical Background

The recent widespread introduction of high power level, high power density, and high operating temperature devices such as rocket motors and nuclear reactors with their inherent capability for rapid transient power level changes has placed an increasing demand on the fundamental investigation of high temperature, high flux, rapid transient heat transfer processes, and mechanisms. The desirability of increasing further both the operating temperatures and thermal flux levels for such devices has generated very large research efforts in boiling processes, liquid metal heat transfer mechanisms, and heat exchange to fluids in complicated flow regimes, e.g., swirling or vortex flow with sub-cooled boiling. The use of ohmic electrical heating to simulate the actual power source in fundamental laboratory research has long been accepted practice. However, the low bulk metal resistivity in combination with the relatively large mass and volume of the engineering shapes of interest, e.g., coolant tubes and flat fuel plates, dictated the use of very large currents at relatively low voltage in order to simulate the rapid transient response, high flux, and high temperature capability of these new power sources. These high current power systems are bulky, expensive, and difficult to control. In addition, such problems as the contact resistance being almost equal to the heater resistance, the inability to measure accurately the heater voltage and current, and the inability to monitor accurately the heater surface temperature, all suggested that a new heating system was required for laboratory scale studies.

Winding and co-workers (1) and (2), in 1955 and 1956 suggested that thin metal films of significant surface area and high electrical resistance might be useful as simultaneous resistance thermometers and heating elements in thermal transport studies. Fleming (3) so utilized thin gold films deposited by means of gold paste on the inner surface of cylindrical substrates in a burnout heat transfer study to water in swirling flow. His results were not in agreement with those of a similar study using more conventional heating elements conducted by Gambill (4). The differences in the results of the two studies were not fully resolved in terms of the transport mechanisms involved, or Fleming's interpretation of his own data. In short, Fleming's work suggested the need for high-speed, precision instrumentation in such studies and more fundamental data on thin film behavior whenever they were to be employed as simultaneous resistance thermometers and heating elements.

Bomar (5) subsequently developed the high-speed, precision instrumentation suitable for transient thin film studies and utilized vacuum vapor deposited nickel films on flat fused quartz substrates for a transient, sub-cooled pool boiling burnout study with water. The film quality and uniformity distribution in Bomar's work were thought to be greatly superior to that of Fleming's due to the superior plating and environmental control possible in the vapor deposition process. Even so, the burnout data of Bomar were in disagreement with the bulk of the literature in that apparent film temperatures were too high and apparent film fluxes were too low at burnout. This bore the same relationship to the literature data as Fleming's data, i.e., fluxes which were apparently too low and film temperatures apparently too high at burnout. Bomar attributed his disagreement to film

thickness anisotropy as a result of the tendency of nickel to alloy with its plating filament during deposition.

Purpose of This Research

The purpose of this research was to ascertain and reveal any intrinsic properties of thin metal films that would limit their usefulness as simultaneous resistance thermometers and heating elements for high temperature, high flux, transient studies involving fluids, phase changes, and/or complex flow geometries. It was obvious from the results of the above mentioned applications of thin metal films that film thickness uniformity was one variable that needed to be considered. Fleming had suggested that for physical systems similar to his, film metal melting temperature and film adherence to the substrate were critical factors. In order to encompass a suitable range of these and other properties, such as thermal and electrical conductivity, temperature coefficient of resistance, etc., the three face centered cubic metals, copper, nickel, and aluminum were chosen for comparative analysis.

In order to avoid any complications arising from phase changes or transport to the ambient environment and to test only intrinsic film properties, the testing of the films in the insulated and inert environment of a vacuum seemed a reasonable approach. High-speed precision instrumentation similar to that of Bomar was used to monitor film behavior throughout each test.

In short, the investigation was designed to answer the following questions: Do intrinsic properties of thin metal films deposited on nonconducting substrates limit the usefulness of these films as simultaneous

resistance thermometers and heating elements in transient, high flux studies? If the answer to this question is yes, what factors are important and how do they influence film performance in such a role? What can be done to overcome any difficulties in order to permit the successful and reliable use of such films in future studies? As a result of the study design, data on the extent of film-substrate thermal interaction, and the maximum operating limits for films of the three chosen test metals under the most restrictive thermal transport conditions possible were obtained.

Related Literature

With the exception of the previously discussed works of Fleming (3) and Bomar (5), the adaptation of thin metal films as simultaneous resistance thermometers and heating elements in transient thermal studies has not been extensive. Kirby and Westwater (6) used conducting films on glass as resistance heaters for a photographic study of bubble formation in nucleate boiling. The coating was not used as a resistance thermometer, however. No comprehensive intrinsic limitations study for films of large surface area were found for direct comparison with the results of this investigation.

On the other hand, the technology of thin film applications for decorative purposes, for optical uses, and for electronic circuit components is abundant in the literature. The best general survey is the work of Holland (7). The possible use of thin films of several metals as area monitoring resistance thermometers was investigated by Winding, et al. (1) and (2), who applied such films for the measurement of heat transfer coefficients in condensing liquid systems. Others have used thin film resistance thermometers in shock-tube experiments (8), aerodynamic heating studies (9),

and as thermal flow detectors (10),(11), and (12).

General film characteristics and thermometric properties when exposed to external heating have been extensively examined in the works of Belser, et al. (13),(14), and (15). The results of Cnare (16) with exploding foils, and Chace (17) with exploding wires in vacuum were available for comparison between the effects of high energy, very rapid heating and the relatively low energy, low heating rates utilized for the films in this work.

CHAPTER II

EXPERIMENTAL INSTRUMENTATION AND EQUIPMENT

General

One of the major objectives of this study was the establishment of the intrinsic limitations of thin metal films as rapid transient, high heat flux resistance heating elements. In order to reduce the number of heat transport modes to only those characteristic of the physical system, namely radiation to the ambient, substrate conduction, and electrical contact end loss, it was decided to test the films in a high vacuum environment. Since it was deemed necessary to make these evaluations under operating conditions similar to those to be experienced in a variety of proposed, transient, high flux studies, the use of a variable power supply coupled with high speed instrumentation techniques were dictated. This desire to test under conditions compatible with and comparable to that of Bomar (5), plus the practical consideration of equipment and support resources availability, suggested that a coordinated attempt be made to develop an experimental setup flexible enough to serve conveniently the needs of both investigations. The resulting experimental instrumentation and equipment as developed and applied for this study are presented in this chapter.

Data Recording System

The heart of the high speed instrumentation was to be a Minneapolis-Honeywell, Series 3170, FM Magnetic Tape Recording and Reproducing System.

This recorder, pictured in Figure 1, was capable of recording two simultaneous electrical signals at 60 inches per second and reproducing these signals on playback at a speed of 0.3 inch per second. This capability effectively expanded by a factor of 200 the time over which the transient data were recorded upon playback, thereby greatly facilitating subsequent data withdrawal and analysis.

Physically, the Series 3170 recorder consisted of a tape transport (deck), two frequency modulated (fm) recording oscillators, two fm signal discriminators, a signal preamplifier, and a variable voltage signal attenuator. Should it have been required, two additional recording oscillators could have been added and four simultaneous channels of data recorded. Record-to-playback speed ratios less than 200 could have been used since the tape transport could be operated at several recording speeds less than 60 inches per second, and the plug-in components necessary to adjust the recording oscillators and signal discriminators for each of these slower recording speeds were readily available from the manufacturer. Because recording short time events (rapid transient processes) were of interest, only the maximum record-to-playback speed ratio of 200 was utilized.

In order to understand some of the difficulties encountered in the thermal tests, particularly for aluminum films, a discussion of the operation and limitations of the recording unit must be presented. Figure 2 is a schematic diagram of the recording unit as it was utilized in this study. When no signal was applied to the recording oscillators, they generated a "center frequency" of 54 kilocycles. When an information signal in the form of a voltage was applied, the "center frequency" was in-

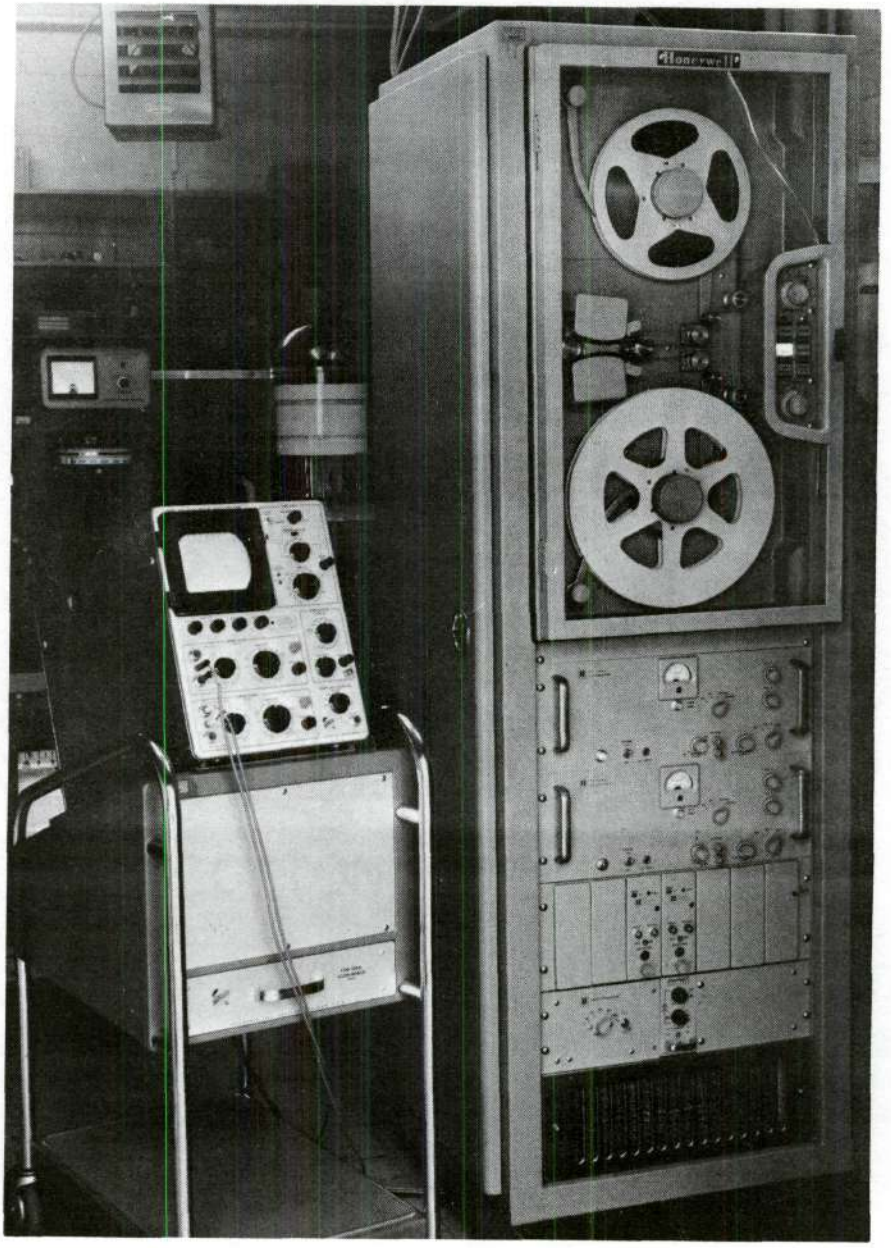

Figure 1. FM Magnetic Tape Recording System and Dual Beam Oscilloscope

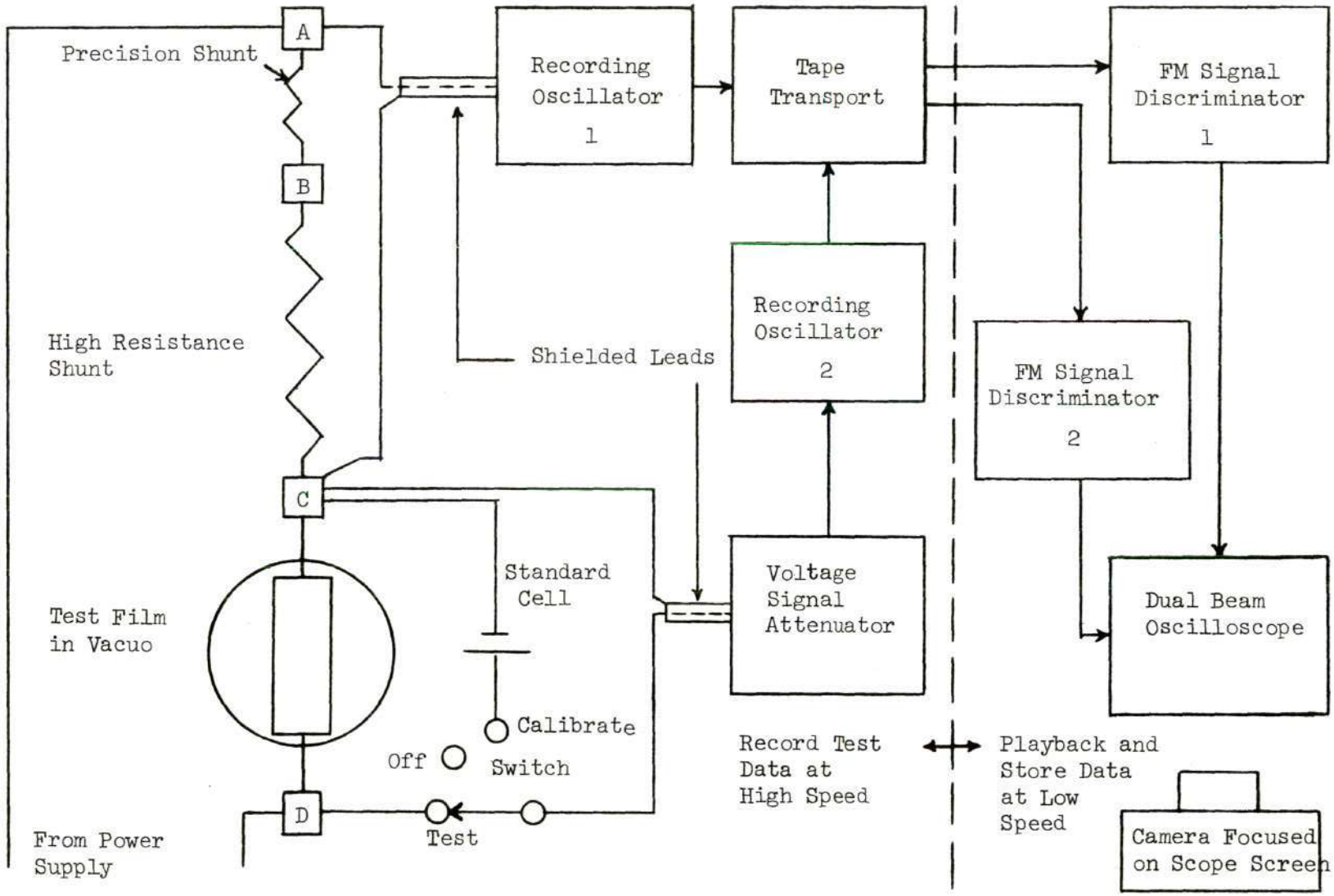

Figure 2. Schematic Diagram of Data Recording and Storage System

creased (for negative voltage) or decreased (for positive voltage) by an amount proportional to the magnitude of the impressed voltage. The maximum recordable signal for these oscillators was 1.2 volts.

To record the voltage drop across the test film, the signal had first to be reduced to a recordable level by the signal attenuator. This attenuator consisted of a set of precision resistors, arranged in a simple voltage divider circuit, mounted on a rotary switch so that either a 5, 10, 25, 50, or 100 volt maximum input (film) voltage could be recorded without overloading the recording oscillator. It was desirable to utilize as much of the total oscillator capacity as possible in each test from the standpoint of data retrieval accuracy and sensitivity. Therefore, the attenuator setting preselected for each trial was in reality a guess of the smallest voltage, chosen from the above set of available voltages, that would exceed the maximum voltage to be applied to the film during the course of that trial. With only very limited previous film behavior and trial data available as a guide in each selection, it was not surprising that partially recorded tests as a result of under-attenuation were experienced. Copper and nickel films performed consistently enough so that this was not a major problem, but the sporadic behavior of aluminum films caused the complete loss of several tests, and the reporting in this work of additional partial recordings.

Original plans for measuring the film current called for the recording of the voltage drop across a precision, low resistance shunt placed in series with the test film. This low voltage signal was to be amplified by the signal preamplifier before being fed to the current channel recording oscillator. However, severe difficulties with the signal pre-

amplifier voided this approach. Based on the current capacity of the rectifiers used in the power supply, plus an estimate of the maximum current capacity of the films to be used in this investigation, a nominal value of 60 amps was judged to be the greatest current likely to be encountered by the recording system. Equating the 60 amps with the 1.2 volt maximum recordable signal on the recording oscillator suggested that as an alternative to the use of the signal preamplifier, the film current might be measured by directly recording the voltage drop across a shunt of approximately 0.02 ohm wired in series with the test film. Since the entire recording system was to be calibrated immediately prior to each test, the precise value of the shunt resistance chosen was not critical. On the other hand, the constancy of this resistance throughout each test was of paramount importance if the calibration parameters were to be applicable to the in-trial data.

Due to the relatively high shunt resistance required, it was felt that ohmic heating during the course of a film test might result in unacceptably large resistance changes in a shunt resistor of conventional design. Consequently, a special shunt was fabricated to minimize the temperature increase of the shunt due to ohmic heating and thereby to stabilize its resistance throughout each experiment. The special shunt consisted of a large diameter, solid copper wire cut to the appropriate (very long) length required to give a resistance of approximately 0.02 ohm. The wire was formed into a few, very large loops by winding it around the circumference of a wooden table, the loops being separated a minimum of two inches from each other in order to minimize the introduction of any induction component into the test circuitry. This shunt which possessed

large mass, large physical dimensions, low resistivity, and high thermal conductivity, should yield low thermal volumetric generation rates, small thermal gradients, and small overall temperature increases when subjected to pulsed ohmic heating of the magnitude involved in this study. The special shunt and its application for film current measurement is illustrated in Figure 2 as the resistance between taps B and C. The resistance shown between taps A and B of Figure 2 was a very low resistance precision shunt used in conjunction with the Mallory Voltage Reference Battery 303113, also shown in the diagram, for calibration of the recording system. The calibration procedure is described in detail in Chapter III.

Through the use of the devices just described, satisfactory film voltage and film current histories were readily recorded. In order to withdraw these data from the tape and store it for convenient analysis, the following equipment and techniques were required. The first step was the simultaneous playback at 1/200th of the recording speed of the two recorded channels, one each through the two fm signal discriminators. These discriminators sensed the displacements from the new "center frequency" of 270 cycles caused by the recorded signals, and converted these displacements to voltage outputs proportional to the amount of displacement in each case. The voltage outputs were fed to a Tektronix, Model 502, Dual Beam oscilloscope for simultaneous visual display.

Photographic storage was successfully accomplished through the use of a Kodak Retinette camera fitted with a plus 3, close-up lens. The camera was mounted on a tripod and fitted with a cable release to insure stability during the time exposures required to photograph a scope sweep. The camera was prefocused on the scope screen using a ground glass slide

in the film plane, and the settings so obtained were used for all measurements. Proper lens-to-scope screen position from picture to picture and trial to trial was assured through the use of a positioning template. This template was cut to fit over the scope screen and camera lens when the correct distance and alignment were achieved. Properly exposed 35 mm negatives of the scope traces were easily obtained in a semidarkened laboratory environment utilizing normal scope spot and grid illumination intensity, a scope sweep rate of 5 cm/sec (approximately two seconds per sweep), an f:8 lens setting, and a slow film, Kodak Panatomic -X. A typical photographic data exposure may be seen in the bottom picture of Figure 3.

In addition to the basic system just described for recording, displaying, and storing the film voltage and current time-histories, two continuous supplemental thermocouple measurements were also made. One platinum:platinum -13 per cent rhodium thermocouple was pressed against the side of the substrate immediately beneath the film, midway along its length. This thermocouple was connected via a Conax vacuum feed-through to a previously calibrated Minneapolis-Honeywell-Brown Electronik Potentiometer and Strip Chart Recorder. This system was activated prior to each test and used to provide a continuous monitor of the substrate behavior. This information was considered desirable in regard to the formulation and confirmation of the boundary conditions applied in the film substrate heat transfer analysis presented in Chapter VI.

A second platinum:platinum -13 per cent rhodium thermocouple was suspended approximately 1/16th of an inch over the film center. The thermocouple was connected using the other Conax feed-through to a precali-

Ideal 3-phase bridge rectifier DC voltage output

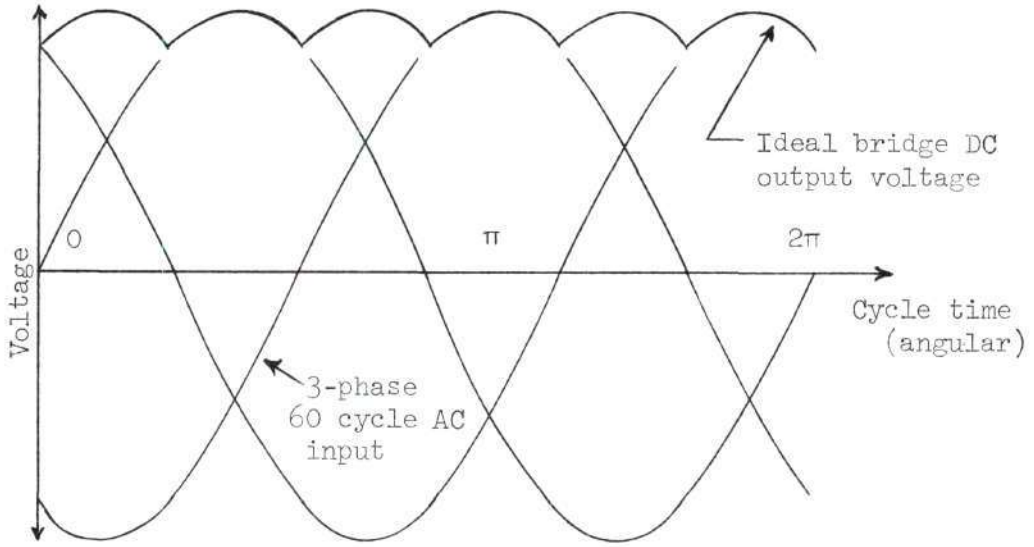

Typical film voltage and film current data traces

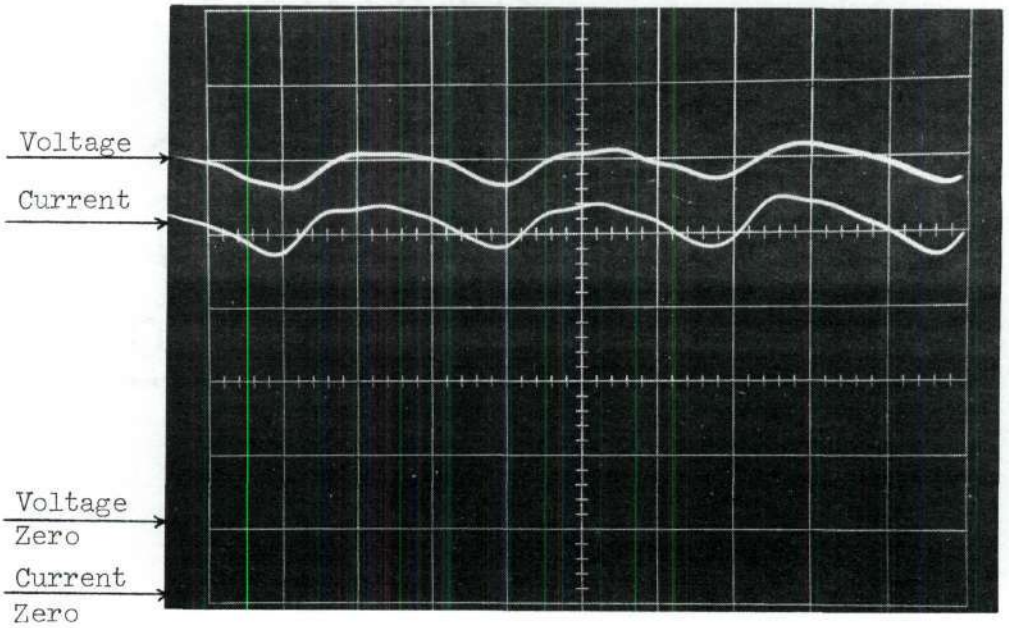

Note: The 2 second scope scan time equals approximately 1/2 the 60 cycle period yielding the 3 DC ripples

Figure 3. Ideal 3-Phase Bridge Rectifier Output and Typical Film Voltage and Current Trace

brated Wheelco, Model 8000, Strip Chart Recorder. This system was also activated prior to each trial in an attempt to provide some estimate of the thermal effects accompanying the pressure surge and various electrical phenomena observed at the moment of film failure.

Film Test Power Supply

In order to make possible an analytical treatment of this problem comparable with the measured data, it was decided that only direct current (dc) heating would be employed. Fleming's work (3) indicated some of the difficulties, both experimentally and analytically, in the interpretation of the data when alternating current (ac) heating was employed. Bomar (5) subsequently verified some of these difficulties, even when using sophisticated instrumentation techniques.

Since the major objectives of this work included the delineation of the limitations in the use of thin film elements and the investigation of the mechanisms attributing to these limits, it was thought that the added complication of substrate damping interactions with the attempt of the film to follow a cyclic driving function could only serve to confuse rather than to clarify the results. Indeed, the sensitivity of the available instrumentation would not permit an accurate assessment of the temperature pulse experienced by a film during one cycle of ac operation, and therefore, any average cycle values measured corresponding to film failure would be unrepresentative of the real failure conditions by an undetermined amount. In addition, any attempt to supplement analytically the data that could be obtained using ac heating would not be justified due to the large experimental errors and severe analytical complexity. It

appeared quite reasonable that the use of dc heating would provide the maximum amount of useful data and insight into the problem, and that the significant results could be easily applied, at least qualitatively, to ac heating situations.

Initial requirement estimates suggested a capability of variable dc voltage from 0 to 100 volts with a maximum corresponding dc current capacity of 100 amperes. Because of their bulk, cost, and the great difficulty to control and vary their output, storage batteries and dc motor-generator sets were quickly discarded as power source candidates. Since full-wave rectified dc is almost equivalent to ac with regard to the pulsed nature of the film response, the dc system finally chosen would have to be smoother than full-wave rectification or no advantage would be obtained through its use. The best compromise between smoothness and controlability appeared to be a three-phase rectifier bridge. The system which ultimately evolved is shown schematically in Figure 4.

Nominal 220 volt ac, 3-phase line voltage was fed through a master fuse-switch box to a Powerstat Variable Autotransformer, Model 1156D-6Y. This autotransformer, pictured in Figure 5, along with a control box immediately behind the vacuum test chamber, consisted of a vertical stack of six transformers connected to a common, manually operated control shaft. Two transformers and a load balancing choke were connected to each incoming voltage leg in a 3-phase wye hook-up. The autotransformer output was variable from 0 to 280 volts, current from 0 to 90 amperes, at a maximum kva rating of 43.6.

The transformer output was fed to a bridge rectifier which consisted of six Sarkes-Tarzian, No. 30T3N, silicon rectifiers wired as indi-

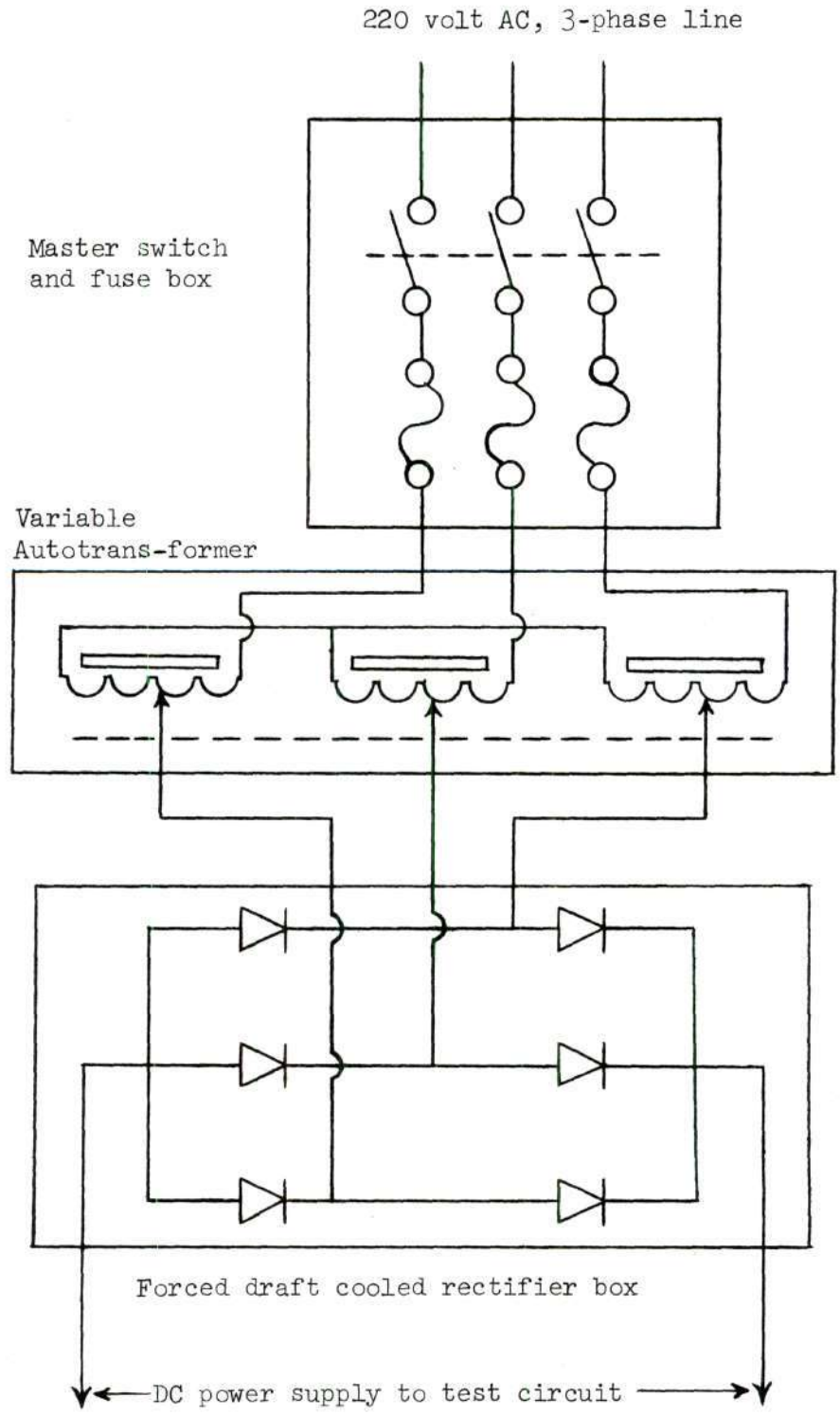

Figure 4. Schematic Diagram of DC Power Supply

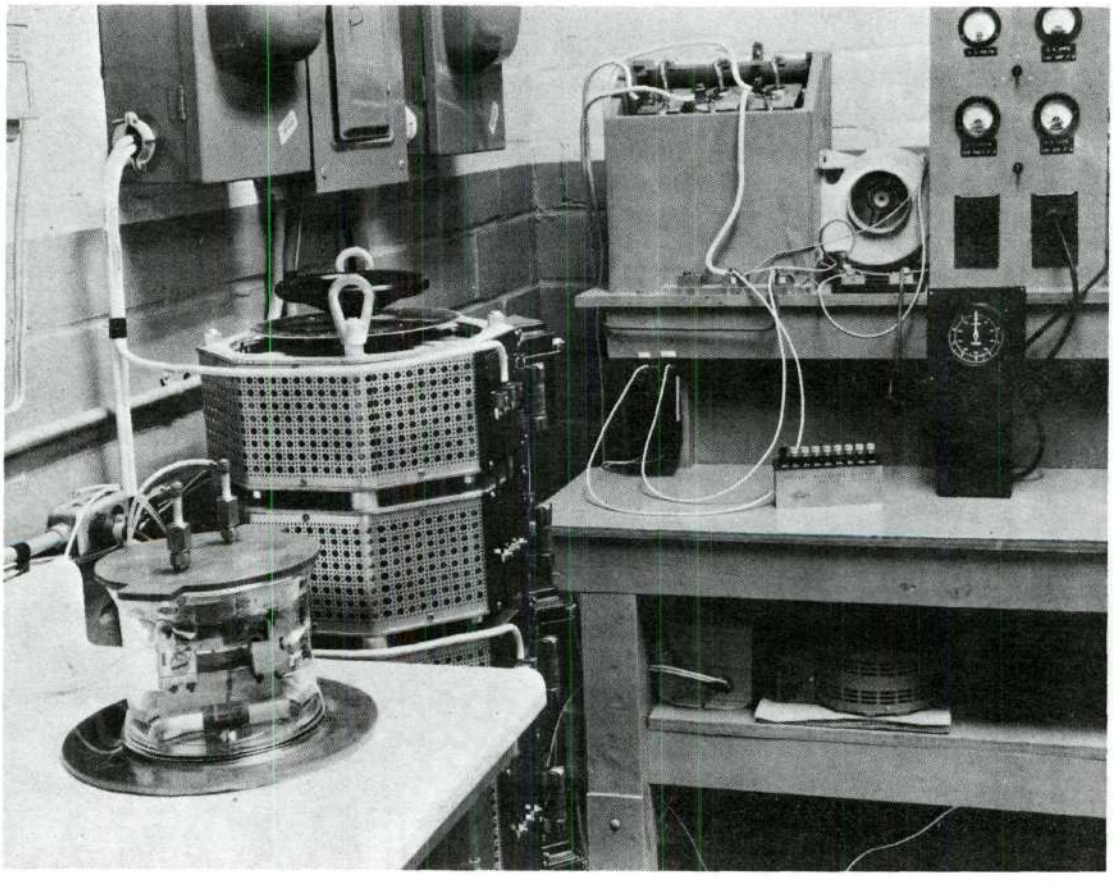

Left to right: Vacuum test/plating system rigged for film test, powerstat autotransformer unit with fuze-switch box above; experimental instrument bench - upper bench level left to right: rectifier box and blower, takeoff taps, calibration shunt, meter-power convenience panel - middle bench level left to right: switch assembly, Mallory standard battery, electronic timer - lower bench level: plating power supply.

Figure 5. Panoramic View of Set-Up Film Test Vacuum Chamber, Power Supply, and Instrument Work Bench

cated in Figure 4. These rectifiers were mounted on aluminum bar heat sinks, which in turn were installed in a forced draft cooling box. The resulting rectifier box is pictured in Figure 5, mounted on the upper left corner of the instrument work bench. The rectifier cooling precautions were taken to reduce the chance of thermal damage to the rectifiers should it become necessary during the course of a film test to exceed the rated rectifier current of 50 amperes. A maximum dc output of 140 volts was available from the bridge without exceeding the peak inverse voltage rating of the rectifiers. Both the current and voltage capacities of the bridge proved more than sufficient for the tests conducted in this study.

Figure 3 presents a sketch of the ideal bridge output wave form, and for comparison a picture of a typical test trace showing the actual output wave form and corresponding film response. Proper injection of the bridge output into the test circuitry is indicated in Figure 2. Figure 3 clearly indicates that the dc ripple frequency is six times the supply frequency and has no zeroes. The variation about the mean voltage during a given supply cycle is seen to be relatively small, and therefore cycle or half cycle average voltages and currents will have significant meaning as related to average film temperature.

Figure 5 presents a panoramic shot of the entire test power supply as wired for an experiment. Included in the picture is the test chamber with film and film holder in place, the autotransformer unit with its master switch-fuse box above it, and the experimental instrument work bench. Mounted on the upper level of the bench from left to right is the rectifier box and blower, and a convenience panel of ammeters, voltmeters, and 110 volt ac power receptacles. Clearly visible in front of the recti-

fier box blower is the low resistance, precision, calibration, resistor. Other takeoff taps are shown in front of the rectifier box wired with the power supply, the special high resistance current measurement shunt, and the two shielded lead input cables to the data recording system. Visible on the middle level is the switch and standard reference battery used in the calibration of the recording system, and the electronic timer used to time the photographs during data playback and storage. Barely visible on the bottom level of the bench is the power supply used in the film plating operation.

Vacuum Test/Plating System

A high vacuum system was specially designed and constructed which could be alternately used as a vacuum film test and vacuum vapor film plating apparatus. The vacuum vessel itself consisted of a 6-inch diameter by 6-inch long section of Pyrex pipe having standard O-ring vacuum seal grooves on each end. The top of the chamber was a machined and highly polished brass plate fitted with two threaded Conax high vacuum power feedthroughs. The bottom of the chamber was a highly polished brass base plate through which the pump access port was cut. One thermocouple and two small threaded Conax fittings were placed in the pump access port of the base plate.

The silver soldered, heavy walled copper piping was designed with the minimum number of bends and for the shortest possible distance, in order to minimize the line pressure drop. The pumping system consisted of a 2-inch, National Research Corporation water cooled, oil diffusion pump, in series with a large capacity, two-stage mechanical pump. The

piping layout included provision for isolating the diffusion pump while the chamber was prepumped to mechanical pump pressure, 50 microns of Hg, or while the chamber was opened for cleaning, readjustment, or conversion to its alternate function. This basic system with an empty chamber, carefully cleaned, dried, and outgassed, using freshly greased O-rings and fresh mechanical pump oil, produced an ultimate vacuum of 1×10^{-6} mm of Hg. Under typical operating conditions as either a plating or film test system, the vacuum capability was approximately 1×10^{-5} mm of Hg.

The use of this basic system for metal film deposition is illustrated in Figure 6. The Conax fittings in the top of the chamber were used both to support and to feed power to the 0.02 inch diameter tungsten plating filament. The filament shape shown in Figure 6 was used to minimize filament buckling due to thermal expansion. Reduced buckling aided the production of uniformly thick films and helped prevent breakage of the filaments as they became increasingly brittle during the course of the plating process. Power was supplied to the filament using a hand operated, Standard Electric Company Adjust-A-Volt Varic Transformer in conjunction with a step-down transformer. The resulting ac filament voltage was variable from zero to sixteen volts with very fine control.

For the plating operation a substrate outgassing heater was mounted in the vacuum chamber, as pictured in Figure 6. The heater was constructed by bending copper sheet metal to form a side and bottom radiation reflector, and fitted with a grooved nickel top plate upon which the substrate rested. Heat was supplied from tungsten heating wire, wrapped around two alumina rods running down the middle of the reflector chamber. The two ends of the chamber were closed by silver soldered copper plates into which holes were

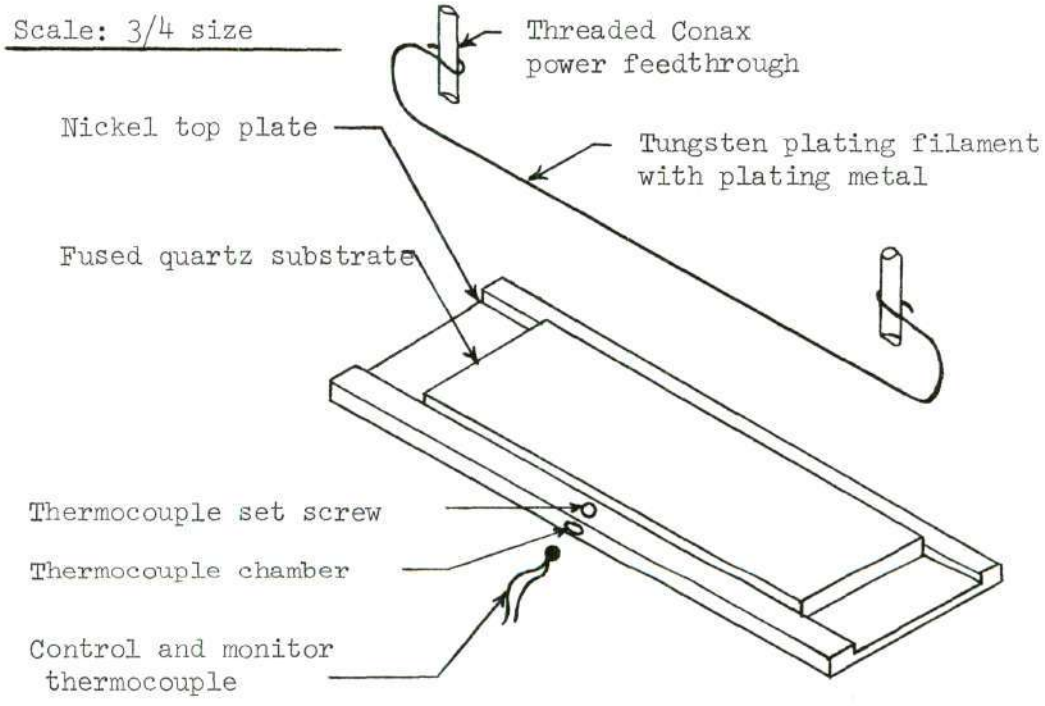

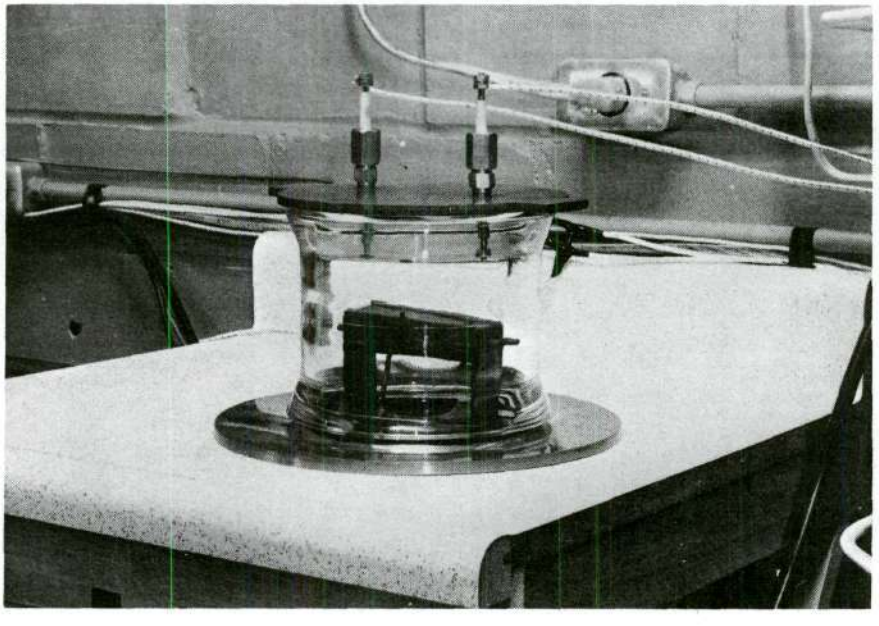

Figure 6. Vacuum Chamber Set-Up for Film Plating Operation with Detail of Substrate-Filament Geometry and Instrumentation

drilled to provide support for the alumina heating elements. The copper end plates were cut to a length sufficient to place the substrate at the desired distance from the plating filament.

Power was fed to the substrate heater through the threaded Conax fittings in the pump access port. Substrate temperature was monitored and controlled by a platinum:platinum -13 per cent rhodium thermocouple fixed to the nickel top plate of the substrate heater by a set screw. The thermocouple output was fed through the Conax fitting in the pump access port to a Brown Pyr-O-Vane temperature controller. The controller operated a relay to turn on or off, as required, a Standard Electrical Products Adjust-A-Volt Variac Transformer the preselected output voltage of which was used to power the substrate heater. The pressure was monitored with a Consolidated Vacuum Corporation Discharge Vacuum Gauge, Type GPH-100A.

The design of the plating system as just described excluded metals with low vapor pressure which could contaminate the substrate during the plating process. The avoidance of the use of rubber tubing and electrical solder, combined with a minimum number of feedthroughs, eliminated flux pockets and intermittant leakage. By taking advantage of the system flexibility, the substrate heating facility, and using the procedures outlined in Chapter III, good quality films of aluminum, nickel, and copper were routinely made.

Conversion of the basic components into a film test vacuum system is illustrated in Figure 7. The picture shows a close-up of the film holder assembly with a test film wired for an experiment positioned in the vacuum chamber. The holder assembly was placed on a ceramic platform to insulate it electrically from the vacuum chamber base plate. The output

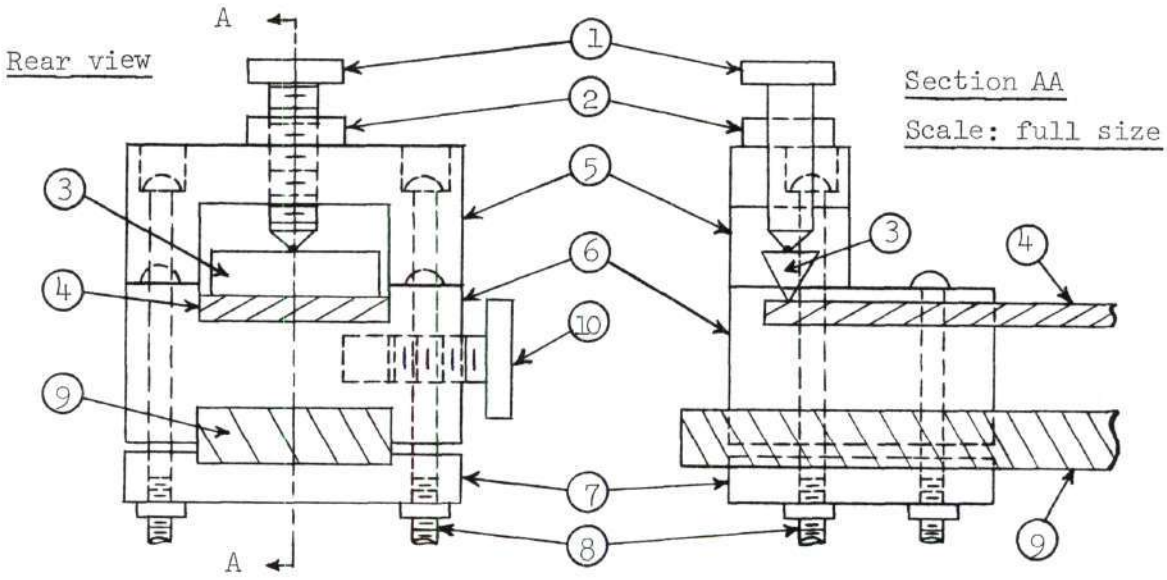

Parts Legend: 1-bridge bolt; 2-lock nut; 3-knife blade contact; 4-plated quartz substrate; 5-arched top section; 6-middle section; 7-bottom section; 8-steel clamp bolts and nuts; 9-ceramic spacer bar; 10-power lead bolt

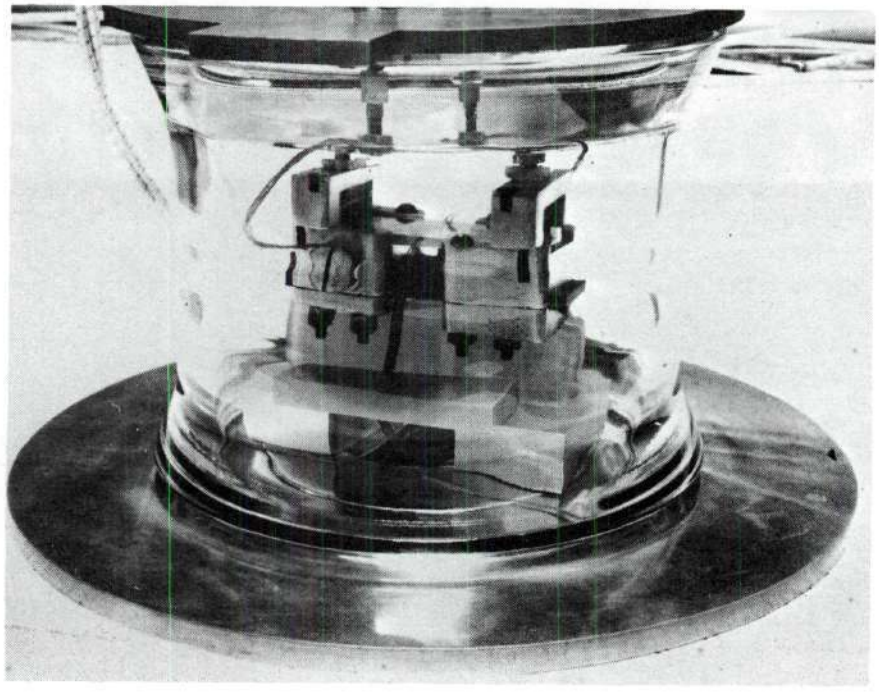

Figure 7. Film Holder Assembly in Test Chamber, Plus Detail Drawing of Film-End Block Assembly Connection

of the experimental power supply, discussed previously, was fed to the film holder assembly through the Conax fittings in the chamber top. The two continuous monitoring thermocouples, one against the substrate and the other immediately above the film, are also shown in Figure 7. The Conax thermocouple fitting in the pump access port was used for one of these monitors, and the two threaded Conax fittings also located in the pump port were used for the other thermocouple.

The film holder assembly mentioned above and shown from the side in the picture of Figure 7 was specially designed and constructed for this investigation as the means of applying electrical power to the films. Early in the planning stages of this study, a literature search revealed many suggested methods for attaching electrical leads to thin metal films. Belser (15) suggested sticking "pig tail" wire leads to the ends of the substrate using platinum, silver, gold, or other metal contact pastes, and then overplating a portion of the end paste zones during the film deposition. Winding (1) suggested a similar technique using overplated metal paste end regions, except that copper pressure plates were used to contact the metal paste zones rather than sticking a wire "pig tail" into the paste itself. Fleming (3) had experimented with contact pressure point leads directly on the film, as well as the use of "pig tail" leads in liquid metal doped or metal contact pasted end sections. Bomar (5) used a liquid gold end layer which was partially overcoated with a silver contact paste. The nickel films were deposited over the unsilvered gold layer, whereas the silvered region was soldered to copper electrical contact blocks using a low melting temperature lead-silver alloy. All of these techniques were considered unsuitable or undesirable for this study

for the following reasons: (1) Any scheme requiring the use of a solder had to be rejected in order to avoid contamination of the test/plating vacuum system with flux or flux residue. If soldering was to be attempted after plating, film oxidation during soldering had to be avoided. If oxidation could be avoided through the use of a low melting temperature solder, then calibration to desirably high temperatures could not be achieved. (2) The use of liquid metal dope or metal paste required severe, high temperature curing to burn out the organic carrier and produce a metallic product. This severe treatment for curing generally resulted in some damage, scratches or knicks to the substrate. In addition, the resulting metal product was porous in nature with an uneven surface, thereby making the required cleaning and drying of the substrate prior to plating very difficult. To this difficulty was added the problem of outgassing the porous network during the plating operation without contaminating the vacuum system with adsorbed water vapor or organic residue. (3) Perhaps the greatest objection to the technique of overplating the film onto liquid metal doped or metal pasted end sections was the nature of the junction between the film and undercoating thus produced. The shadowing action of the undercoating would tend to reduce the amount of metal vapor striking the base of the junction between the undercoating and the quartz substrate. Therefore, the metal film bridge from the undercoating down to the substrate would likely be formed by growth down and inward from the shoulder of the undercoating, and up and over from the floor of the substrate, instead of by progressively filling in the base of the undercoating-substrate junction. Consequently, neither normal film-substrate bond (thermal contact) or film integrity (film tensile strength)

could be expected in the region of undercoating-film juncture. During subsequent cooling of the film from plating temperature to room temperature, the curved film sections in each junction region would be subjected to large thermal tensile stresses. These stresses would possess large force components tending to pull the film outward and away from the base of the undercoating-substrate junction, thereby further weakening the film-substrate thermal contact in this region. The preceding analysis, plus direct observation of Bomar's difficulties with premature junction failures in a boiling water system, showed that some other technique was demanded for an environment where only the heat transfer to the substrate could prevent instant burn-out. The film holder assembly described below in connection with the picture and drawing of Figure 7 was an attempt at such a new technique.

The film holder assembly consisted basically of two identical massive copper end block assemblies joined together by a ceramic spacer bar. The ceramic spacer bar was clamped tightly in a slotted channel between the bottom and middle sections of each end block assembly. The spacing between end blocks could be varied by loosening the steel bolts holding the clamps in place, sliding the end blocks along the spacer bar to the desired spacing, and then retightening the clamp bolts. The middle section of each end block was drilled and taped on opposite sides of the assembled holder for a 1/4-inch fine thread, large-head, copper bolt, specially turned from copper bar stock. These large-head, copper bolts were used to fasten the power leads from the Conax fittings in the vacuum chamber top to the end block assemblies. A slotted seat was cut through the top of the middle section of both end blocks to accomodate the plated

substrate. The third or top section of each end block assembly was a solid copper bridge arching over the substrate seat. These bridges were bolted tightly to the middle sections of the assemblies with sufficient contact surface to insure a good electrical connection. Down through the top of each bridge directly over the substrate center line was drilled and taped a hole for a 1/4-inch, fine thread, copper bolt. These specially turned copper bolts were fitted with copper locking nuts in order to insure good electrical contact between each bolt and its bridge. The end of each bridge bolt was shaped into a polished copper bead.

Electrical contact between the film surface and the end block assemblies was accomplished through the use of soft, solid copper knife blades fabricated for this purpose. Both knife blades were made in the shape of a wedge with the flat top surface and knife edge of each blade polished with extra fine alumina paper. The end block assemblies were prespaced according to the substrate length so that the tips of the bridge bolts were within 1/8th of an inch from each end of a properly positioned substrate. The blade was used by placing its knife edge gently on the film parallel to the substrate end, centered directly beneath a bridge bolt, and screwing down the bridge bolt until light contact was made with the blade top. Utilizing extra care to avoid movement of the blade, the bridge bolt was tightened to provide, simultaneously, high pressure electrical contact between the film and knife edge, and between the beaded end of the bridge bolt and the blade top. The contact was secured by tightening the locking nut on the top of the bridge. With experience, care, and patience, this technique could be employed routinely to produce low resistance electrical connections to thin metal films with a minimum of

film damage.

At first glance the design of the film holder assembly just described and illustrated in Figure 7 may seem overly massive and cumbersome. However, copper was chosen to reduce to a minimum the lead resistance, and to provide a high thermal conductivity platform for the calibration operation. The use of all copper components in the electrical connections avoided any differential thermal expansion effects which could have otherwise altered the connection during the high temperature calibration cycles. In addition, the use of a copper bridge structure with steel constraining bolts for each end block dictated that upon heating the ensemble each knife blade would come under a slight compression, thereby insuring the electrical connection integrity during the calibration process. In retrospect, the design proved not only sound but very flexible for the study at hand.

Temperature-Resistance Film Calibration System

The equipment used to calibrate each film as a resistance thermometer is shown in Figure 8. The foreground in this figure shows from left to right the Rubicon Instruments, Model 1071, Wheatstone Bridge which was used to measure accurately the film resistance, the Rubicon Instruments, Model 2745, Potentiometer which was used in connection with two platinum:platinum -13 per cent rhodium thermocouples to monitor and obtain the film temperature corresponding to a given film resistance, and the film holder assembly which was used as the film electrical connection vehicle during calibration. The background of this photograph displays, from left to right, the calibration furnace temperature control panel, and

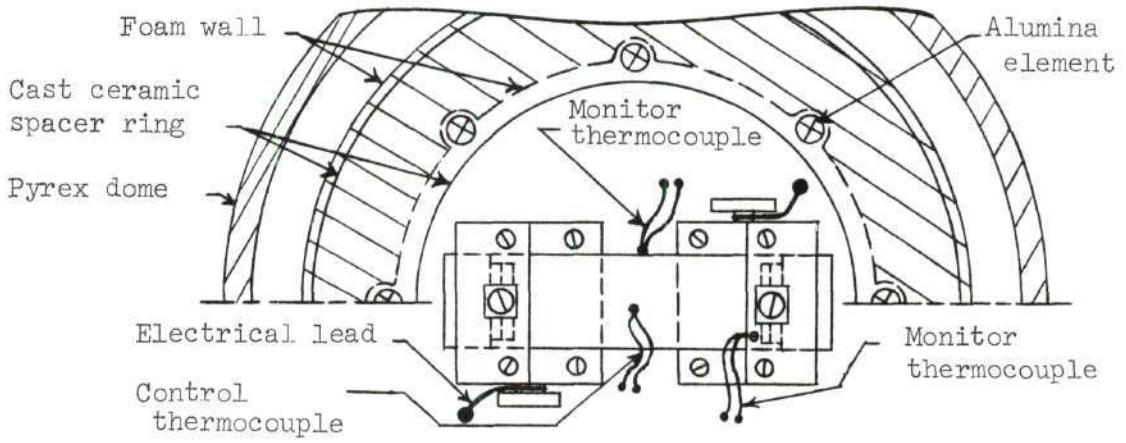

One-half scale partial top view (upper plate removed) of vacuum calibration furnace with film holder assembly in place

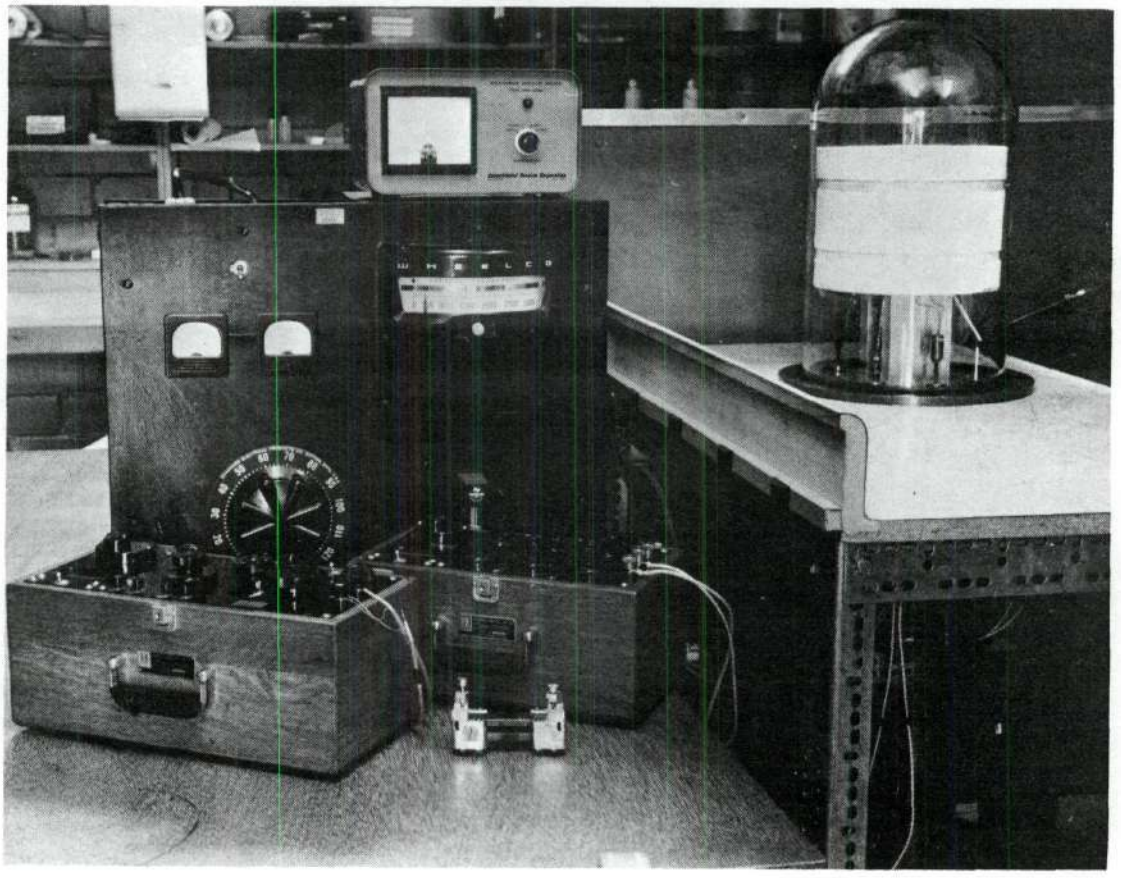

Figure 8. Temperature-Resistance Film Calibration System with Partial Top View of Vacuum Furnace

the vacuum calibration furnace assembled atop its vacuum system support table.

The calibration furnace temperature control panel contained a Wheelco Temperature Controller, Model 402, which was used in conjunction with its own platinum:platinum -13 per cent rhodium thermocouple within the furnace cavity to provide rough film temperature control during calibration. The controller acted by driving a relay which, on demand, placed a pre-selected output from a Standard Electrical Products Adjust-A-Volt Variac Transformer across the calibration furnace heating elements. The relay, power transformer, and heating element monitoring ac ammeter and voltmeter were also mounted in the panel. Mounted on the top shelf of the panel was a Consolidated Vacuum Corporation Discharge Vacuum Gauge, Model GPH-100A, to monitor the calibration furnace pressure.

The vacuum calibration furnace, pictured in Figure 8, was specially constructed to provide the inert envelope required for the three easily oxidized metals tested in this study. The piping and pumping systems were similar to that of the plating/testing vacuum system previously described. The vacuum chamber was an 8-inch diameter by 15-inch tall Pyrex dome. The dome was sealed to the brass base plate with a large, rubber vacuum gasket, greased with Silicone vacuum grease. With the furnace in place, the cleaned system with fresh pump oil was capable of a room temperature vacuum of 1×10^{-5} mm of mercury. Under typical elevated calibration temperatures, the vacuum capability was reduced to approximately 1×10^{-4} mm of mercury. If desired, the dome could be evacuated and back-filled with argon from a high pressure bottle for calibration under one atmosphere of an inert gas.

The furnace itself was unique in that it was constructed of foamed

fused-silica. The furnace cavity was 6 inches in diameter by 4 inches in height with a wall thickness of 1 inch. The end caps were $1\frac{1}{2}$ inches thick. The furnace rested approximately $3\frac{1}{2}$ inches above the base plate on two aluminum blocks placed on either side of the pump access port. By raising the furnace in this fashion, the rubber vacuum gasket was protected from the deteriorating effects of high temperature.

Heat was supplied to the furnace by eight vertical heating elements, equally spaced around the perimeter of the furnace cavity and each recessed into the cavity wall. The heating elements consisted of 1/4-inch diameter by 4-inch long alumina rods wrapped with 0.04 inch diameter Kanthal A-1 resistance heating wire. The elements were spaced and supported at each end by specially cast $\frac{1}{2}$-inch thick ceramic spacer rings. These rings were sandwiched between each foam end cap and the foam cylindrical center section of the assembled furnace.

Permanently positioned through the furnace bottom were the three platinum:platinum -13 per cent rhodium thermocouples, the bare copper wire electrical leads to the film holder assembly, and the furnace heater wire leads. The two temperature measuring thermocouples were fed through Conax thermocouple vacuum fittings in the base plate to the potentiometer. One of these thermocouples was positioned against the side of the plated substrate midway along its length. The other was attached to the bridge (arch) section of one of the film holder end block assemblies using a drilled-seat set screw arrangement similar to that illustrated in the drawing of Figure 6 for the top plate of the substrate heater. The temperature controller thermocouple was suspended about 1/8-inch over the film center. Its output was fed through the base plate using two of the six available

threaded feedthroughs. Two each of the remaining four threaded feedthroughs were used for the furnace heater power and film electrical leads, respectively. The partial top view drawing of Figure 8 illustrates the heating element design and support as well as the thermocouple and film holder positioning. The photograph of Figure 8 shows the furnace exterior, including the three foam sections, the two ceramic spacer rings, the furnace support blocks, one of the furnace power leads, and one of the measuring thermocouples. It had been suggested that the use of the dusty, abrasive and very porous foamed fused-silica furnace might result in unduly large pumpdown times and other vacuum system operational difficulties. However, by using compressed air to blow out thoroughly the foamed product prior to installation, dust problems were completely avoided. By pre-outgassing the furnace cavity at 1400-1600°F for several hours under vacuum prior to its use as a calibration furnace, all residual organic material and other adsorbed gases were boiled out of the foam matrix. When the piping system was subsequently cleaned, the diffusion and mechanical pump oil changed, and the outgassed foamed fused-silica matrix kept under mechanical pump vacuum when not in use, pumpdown time was reduced to and held at acceptable levels. The design ultimately proved very sound, since cyclic operation up to as high as 1600°F at 3×10^{-4} mm of mercury produced no damage in the furnace structure, its windings, the dome, or any other component of the vacuum system. By utilizing the temperature controller to establish a rough temperature level, followed by a slight hand manipulation of the furnace power, a very flat temperature profile could be obtained in the furnace cavity. This capability plus the procedure described in Chapter III resulted in high quality thermometric data for the films tested in the investigation.

CHAPTER III

EXPERIMENTAL PROCEDURES

The following description of the experimental procedures and techniques that evolved from and were used for this study will clearly support the contention that any investigation utilizing thin metal films is as much art as it is science. Though it was quite true that every effort was made to benefit from other investigations, particularly through personal contact with Mr. Belser, Dr. Fleming, and Dr. Bomar, the final procedures were generally those arrived at through a trial and error process. Each procedure described in this chapter was proved workable within the manipulative ability of this investigator and within the limitations imposed by the experimental environment and the available instrumentation. Indeed, it may be stated that the successful establishment of a workable experimental technique, coupled with the design and construction of the various special equipment demanded by it, was in itself a major accomplishment of the research program.

The presentation of the complete processing of an experimental film from production through data reduction will serve not only to present the established experimental procedure, but also to indicate why so much time and effort had to be expended for each trial even though the maximum running time for any film was well under one minute.

Thin Metal Film Production

One of the main interests in thin film research for heat transfer

applications arises from the hope that if they can be made sufficiently thin, they will possess significant electrical resistance while at the same time providing a large heat transfer surface area. Such a combination of properties would then permit the use of conventional, low cost voltage sources to produce high thermal fluxes at easily manageable currents for laboratory heat transfer studies. Obviously, the key to a successful realization of such an application lies in the ability to produce high quality, uniform, metal films in a routine operation that permits at least reasonable thickness control.

Many methods are discussed in the literature for metal film production. Candidate methods included electrochemical polishing of a thin slice of bulk metal, the use of liquid metal dope or pastes, sputtering, chemical plating from a reaction bath, and vacuum vapor deposition. From the standpoint of thickness controlability, ease of production, and quality in terms of the number of mechanical flaws in the film surface, vacuum vapor deposition appeared to be the best choice based on the varied experiences of the other researchers contacted by this investigator. The question of thickness uniformity using vapor deposition was investigated in detail as a supplement to the main study, and the results are presented as Chapter V of this thesis.

Since metal films of the desired thickness are not capable of self support, the choice of a suitable substrate and its preparation for plating must be considered. Ordinary glass microscope slides were tried first but were rejected. These slides proved too fragile to be compatible with the proposed pressure, knife-blade, electrical contact device, as discussed in detail in the previous chapter. In addition, the high calibration

temperature utilized in the film resistance stability tests, as conducted and reported in Chapter IV, precluded their use due to the possibility of substrate softening and distortion under these conditions. As a result, clear, polished, fused quartz substrates in the sizes, 1 inch by 3 inches by 1/8-inch thick, and 1 inch by 4 inches by 1/8-inch thick were chosen for this study.

In order to obtain good film adherence to the substrate, thereby maximizing film-substrate thermal contact, careful cleaning of the substrate prior to deposition was required. The cleaning procedure found to produce the best results was as follows: (1) The substrate was placed in a hot aqua regia bath and allowed to soak for 20 minutes. This removed any metal from prior platings. (2) The substrate was rinsed with distilled water and cleaned with Calgonite detergent, being scrubbed and then soaked. (3) The substrate was rinsed with distilled water and placed in a boiling solution of Fisher Scientific Company RBS-25 cleanser, which is specially designed to remove troublesome organic greases and residue. Following a soaking of 30 minutes, the substrate was rinsed twice with cold distilled water followed by a final rinse in boiling distilled water. (4) The substrate was removed while still hot from the boiling distilled water rinse, quickly dipped into a bath of Merck CP reagent grade methanol, and placed in a dessicator to air dry. The methanol dip followed by air drying in the dust-free dessicator accelerated the drying process and prevented water spot and dust contamination of the clean surfaces during drying.

The dry substrate was removed from the dessicator and quickly placed in the dust-free enclosure of the Mettler, Model B-6, Gram-atic balance and allowed to equilibrate with its surroundings. The substrate was then

weighed to the nearest 0.01 milligram before the substrate was placed on the top plate of the substrate heater in the vapor plating vacuum system for the actual metal deposition.

Film deposition was somewhat influenced by the metal being plated. In all cases, however, the available literature stressed the need for reasonably large deposition rates in order to avoid a laminated, spongy film product. In order to provide these large rates, a short source-to-substrate distance was demanded. The additional requirement of film uniformity then forced the use of an extended source geometry, which, when subjected to the realities of thermal expansion, resulted in the plating filament shape illustrated in Figure 6. Once the tungsten filament had been shaped, the linear section was cleaned with fine alumina abrasive and washed with reagent grade methanol.

For copper and aluminum films, small diameter (approximately 0.01 inch) wires of electrolytically pure metal were cleaned with fine alumina abrasive and washed with reagent grade methanol. The wires were then cut into short lengths (about 1 inch) and wrapped tightly on the tungsten filament, being certain to crimp the ends of each coil tightly to the filament. The number of coils used varied depending upon the desired thickness of the film. In each case, however, the coils were wrapped in such a manner that the entire linear section of the filament was wrapped. The reasons for this wrapping technique are presented in the "Discussion of Film Thickness Uniformity Results" section of Chapter V.

For nickel, the wire wrapping technique was also tried, but rejected as a result of excessive premature filament breakage due to nickel-tungsten alloying. This problem is discussed further in the section of Chapter V

mentioned above. Instead, the nickel was electroplated to the clean tungsten filament from a standard sulfate bath. The amount of nickel electroplated was varied according to the desired film thickness. The plated filament was rinsed thoroughly with distilled water, blown dry with compressed air, and dried in an oven for a short period to remove the adsorbed water vapor.

Once the plating filament was prepared, the filament was positioned in the plating system as previously illustrated, and the system closed and evacuated to the deposition pressure of approximately 10^{-5} mm of mercury.

Deposition was initiated by setting the substrate heater temperature controller to about 900°F and allowing the substrate to reach this temperature level. The plating filament was then outgassed several times by turning up its power supply until the filament and film metal glowed a dull red color, or, in the case of aluminum, to the highest possible temperature before the aluminum started to melt. The substrate was held at about 800-900°F for a period of approximately one hour following the filament outgassing to insure that all adsorbed vapors on the substrate surface were boiled off and removed by the vacuum pumps. This high temperature outgassing of the substrate immediately prior to deposition was found to increase greatly film-substrate adherence and to reduce the number of ultra-fine mechanical flaws (probably due to very fine dust or smoke particles stuck to the substrate surface) in the plated film.

Following substrate outgassing, the temperature controller was reset to the plating temperature appropriate for the metal being deposited. The plating substrate temperatures were 150-250°F for aluminum, 400-500°F for copper, and 700-800°F for nickel. These temperature ranges were established by a trial and error process as giving the best possible adherence

and the best possible surface condition, while at the same time providing the greatest possible temperature-resistance stability over the range of temperatures encountered in the thermal tests. Since the literature abounds with reports of irreversible resistance changes either upon heating of metal films deposited on cold substrates, or whenever the previous maximum temperature in the film thermal history was exceeded, the whole question of film resistance stability and survivalability when subjected to rigorous external thermal cycling was undertaken as a separate study. The results of that study are reported in Chapter IV.

The use of a thermal curing process following deposition on a cold substrate, or as in this study, deposition on a hot substrate to stabilize the resistance-temperature relation of thin metal films was suggested by the majority of investigators in the field. The reason for such a stabilization was generally postulated in the literature to be stress-relieval in the film structure due to increased mobility of lattice vacancies and trapped vapor impurities at the elevated temperatures, which at lower temperatures had kept the film frozen in a highly stressed state. Some investigators further postulated that the temperature-resistance stabilization obtained by thermal curing or hot deposition was due to actual metal recrystallization within the film structure. Microscopic examination of each freshly plated film made during the course of this entire work strongly suggested that the relatively high degree of film temperature-resistance stabilization obtained using the previously mentioned substrate temperature was a result of at least a partial recrystallization of the films immediately following their deposition. This conclusion was reached despite the fact that of the three metals considered, only the copper sub-

strate deposition temperature range lay above, but just barely, the lowest bulk metal recrystallization temperatures reported in Samans (18). The microscopic evidence supporting this conclusion was the consistent observation that films plated below these temperature ranges appeared to possess a mirror-like reflectance of oblique light (except for surface flaws) with little or no evidence of a large grain structure under high magnification. Films plated in the selected substrate temperature ranges invariably showed some evidence of a regularly and widely spaced system of randomly oriented reflecting zones in an oblique light beam with a corresponding microscopically visible system of grain-like clusters scattered throughout the film surface. Films plated at substrate temperatures above these ranges were observed to become increasingly more diffuse reflectors of an oblique light beam with a correspondingly closer spaced, uniform system of grain-like clusters visible under microscopic observation. Additional discussion of possible film metal recrystallization as a result of both hot substrate deposition and high temperature cyclic calibration is presented in Chapter IV.

With the temperature controller holding the substrate at the preselected level, the plating filament power was slowly applied until the metal on the filament started to melt. At this point, the filament power was increased as rapidly as possible to complete both liquefaction and initiate vaporization at the highest possible rate. The actual rate of increase was limited by a tendency to throw molten metal off the filament, but maximum speed was desired to help reduce alloying tendencies with the tungsten while the metal was in the liquid state, and to insure the required high deposition rates. Mastery of this critical phase of the deposition process required both care and practice. Slight increase in filament power

was sometimes required following liquefaction to maintain a high deposition rate from each molten bead on the filament. When the deposition was completed, the filament power was shut off, but the substrate was held at the plating temperature for about five minutes before the controller was shut off and the plated substrate allowed to slowly cool in vacuum to room temperature.

Immediately following removal of the film from the plating system, it was placed in the Mettler balance, allowed to equilibrate with its surroundings, and then weighed to the nearest 0.01 milligram. The film weight was obtained from the before and after weighings, and the weight average film thickness computed using the substrate surface area and the bulk metal density. The final step in film production consisted of a thorough microscopic examination of the film surface for appearance and quality in order to ascertain its suitability for subsequent testing.

Thermometric Calibration of the Test Film

Upon accepting the production film for further testing, the film was positioned in the film holder assembly as discussed in Chapter II and illustrated in Figure 7. The film holder assembly was positioned in the vacuum calibration furnace, the three thermocouples positioned, and electrical leads connected to the end block assemblies as illustrated in Figure 8. The furnace cavity was closed, the Pyrex dome positioned, and the system evacuated.

Each calibration point was established by first setting the desired temperature on the calibration furnace temperature controller and allowing the furnace cavity to stabilize at this level. The Wheatstone bridge was

balanced at this temperature condition so that only minor alteration would be required for a final reading. The temperature profile was changed slightly within the cavity through hand manipulation of the furnace power supply until the two temperature measurement thermocouples gave identical readings on the potentiometer. At this moment the final Wheatstone resistance measurement was taken and recorded. This resistance value was assumed to correspond to the two temperature measurement thermocouple outputs as read on the potentiometer. The two indicated temperatures from the measurement thermocouples at any given resistance value could generally be manipulated to within $5^{\circ}F$ of one another. The difference between the two temperature-measurement thermocouple readings and the controller thermocouple reading at the time of the resistance reading was less than $30^{\circ}F$ even at the extreme calibration temperatures indicated in Chapter IV. These small temperature differences indicated the flat temperature profile capability of the vacuum furnace.

A complete film calibration history consisted of several calibration points taken both on increasing as well as decreasing temperature cycles. The maximum calibration temperature and the number of calibration cycles were varied according to the film metal and desired test conditions.

In order to be able to correct raw resistance values to actual film resistances at each temperature utilized in a calibration, a blank calibration was performed in which the film was replaced with a massive, flat, solid copper plate. The film holder assembly was used just as if the bar were a plated substrate, and all wiring, thermocouple positions, electrical leads, and operational procedures were identical to a film calibration. The resulting electrical lead and connection resistance-temperature calibra-

tion data are shown in Table 1. Raw calibration resistance values were then corrected to film resistance by substraction of the lead resistance value obtained from Table 1, corresponding to the measured calibration temperature. Typical extended calibration curves for all three metals are illustrated in Figures 10, 11, and 12.

As with the test film production operation, the final phase of thermometric calibration consisted of a thorough microscopic examination of the film surface for condition and quality. The film was not removed from the holder assembly for this examination. A judgment as to the film suitability for thermal testing was made based on the plotted temperature-resistance data stability combined with the microscopic evaluation. If the film was accepted for thermal testing, the holder assembly was placed in the vacuum chamber as illustrated in the photograph of Figure 7.

Data Recording System Calibration

The calibration of the data recording system was performed immediately before and after a film trial to establish and verify the voltage and current scale factors necessary to convert the recorded film voltage and current signals to their actual numerical values. Figure 9 presents the modified test circuitry utilized for calibration. Comparison with Figure 2 indicates that a dummy load of Kanthal A-1 resistance heating wire was used in place of the test film, a known standard dc voltage was recorded instead of the variable applied voltage to the film, and a potentiometer was used to measure accurately the current corresponding to the recorded system current signal by measuring the voltage drop across the precision shunt resistor taps AB in series with the dummy load.

Table 1. Calibration Furnace Electrical Lead and Connection Resistance Versus Calibration Temperature

Calibration Temperature (°F)	Calibration Lead Resistance (ohms)
80	0.0454
120	0.0458
200	0.0456
300	0.0454
400	0.0450
500	0.0450
600	0.0447
700	0.0435
800	0.0430
900	0.0425
1000	0.0420

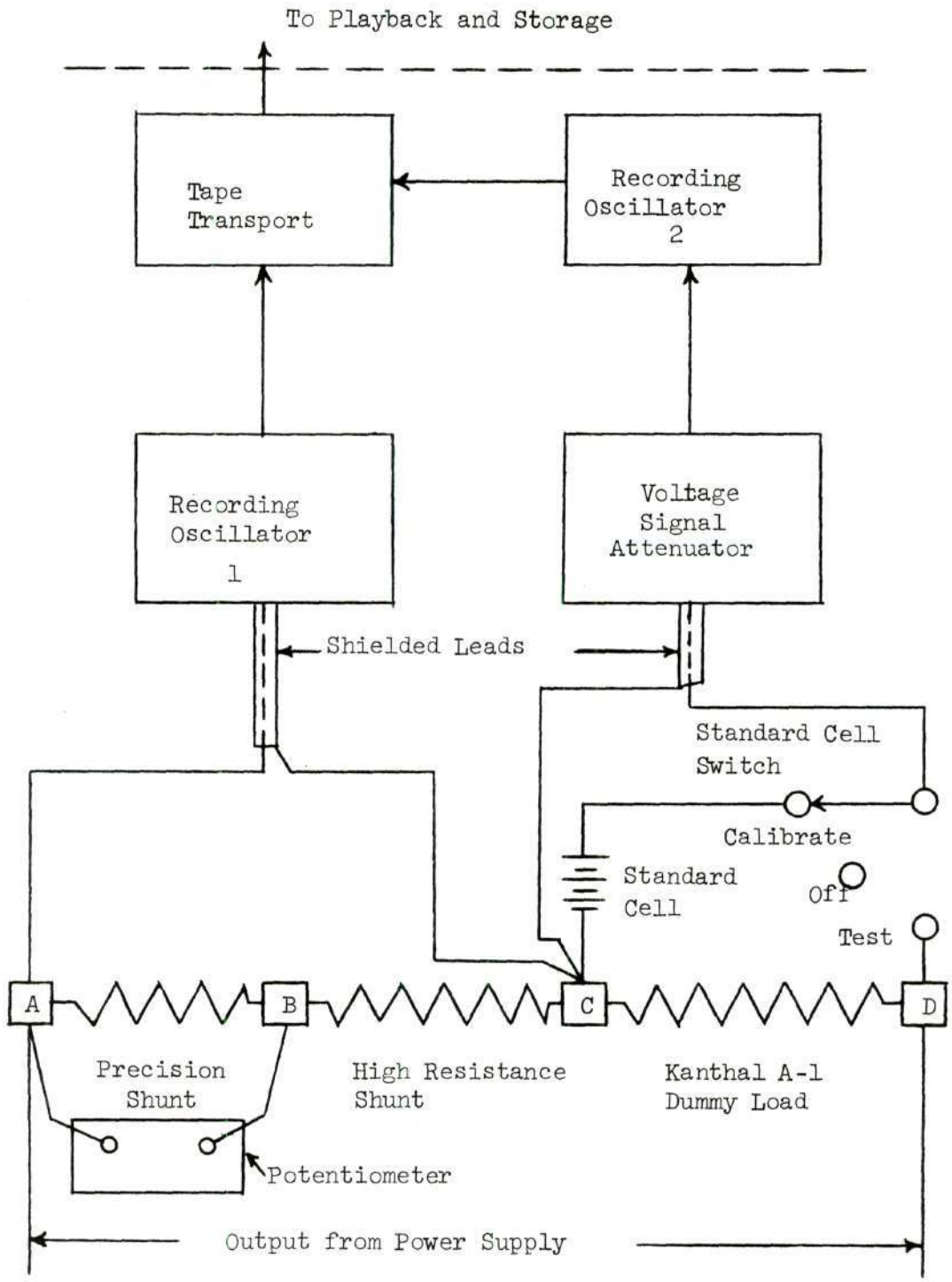

Figure 9. Data Recording System Calibration Wiring Diagram

Mechanically, calibration was accomplished by first allowing the tape unit and oscilloscope to warm a minimum of one hour. The tape deck was activated utilizing the circuitry of Figure 9 with the standard cell switch initially in the off position. The experimental test power supply was used to establish some reasonable rectified dc current flow within the circuit. When the potentiometer output indicated that the current flow was steady, the standard cell switch was turned to the calibrate position and the steady current signal and reference dc voltage signal simultaneously recorded for a minimum of ten seconds. Upon playback, the oscilloscope displacement corresponding to that steady current measured by the potentiometer output was easily established by noting the appearance of the second signal, i.e., the dc reference voltage, on the screen. The two signals were easily identified by the absence of ripples in the dc reference voltage supply. Utilizing this technique, the oscilloscope displacements corresponding to a known voltage and known current were established. The ratios of the reference voltage and measured current to their respective oscilloscope displacements constituted the required data recording system scale factors for each test.

Vacuum Film Tests

After the data recording system calibration, the rewiring to the configuration of Figure 2 was performed. By this time the test vacuum chamber was evacuated to test pressure. Initial temperature and pressure were recorded. The Wheatstone bridge was used to measure the total test load resistance, i.e., the film resistance plus the resistance of the associated power leads. The load resistance was converted by subtraction

of the power lead resistance, 0.1440 ohm, of the film resistance. This room temperature film resistance was compared with the film calibration room temperature value to verify the film condition prior to testing. The test system power lead resistance of 0.1440 ohm had been previously determined by a Wheatstone bridge measurement of the total test load resistance when a plated substrate was replaced by a thick, solid copper bar of negligible resistance.

At this time the discharge vacuum gauge was reset to a higher scale to measure the pressure surge at film failure. The two monitoring thermocouple strip chart recorders were activated, the voltage signal attenuator set, and all last minute adjustments of photographic or other special equipment completed. The master power switch was then closed with the power transformers set to zero voltage output. The tape transport was activated and allowed to reach its proper recording speed of 60 inches per second. Utilizing the hand control wheel on the power supply transformer, voltage was applied at the desired rate to the test film until failure occurred.

From the moment the power was initiated until failure, the trial was approximately timed through the use of a foot-switch activated, Western Electric, Type S-10 Electric Timer. This approximate run time was useful in planning the number and spacing of data storage photographs, as well as aiding in the location of the beginning of the recorded trial following tape rewind. At film failure the maximum pressure surge was observed and recorded. The tape was, of course, stopped immediately after failure and the experimental power supply shut down. The monitoring thermocouple strip charts were also shut off and the maximum temperatures noted. In addition

to these routine actions at or immediately after failure, time exposure photographs of the failure phenomena (in a blacked-out laboratory) were also performed for a few experimental tests. When these initial data retrieval steps were completed, the recording system was recalibrated utilizing the previously described procedure. The fired film was allowed to cool to room temperature under vacuum, and stored under vacuum while the photographic recovery of the taped data was accomplished.

The tape was rewound to the beginning of the pretrial calibration and playback at 0.3 inch per second initiated. During the early playback period when only the carrier signal, i.e., zero calibration current and voltage, had been recorded, the two fm signal discriminators were carefully balanced to the null position. The zero current and voltage signals were then identified, and their base lines set on the oscilloscope grid. When the calibration plateau was obtained, as indicated by the appearance of two signals on the scope, two photographs of the pretrial calibration traces were ordinarily taken. As the playback continued into the early stages of the test run, the discriminators were checked for balance, final base line adjustments made, and a photograph of the zero signal traces taken. The timer was started at the instant either signal was observed to deviate from its base line, and photographs were taken at the preplanned intervals until failure was observed and photographically recorded. Several photographs were ordinarily taken at the region immediately prior to and during film failure in order to ascertain more accurately the failure conditions. One or two photographs were subsequently taken of the post trial calibration traces. The tape unit was then stopped, but left on while several photographs were taken of the failed film and the negatives developed to

insure successful data storage. If the photographic results were acceptable, all systems were shut off. Otherwise, the tape was rewound to the beginning of the pretrial calibration and the entire photographic data withdrawal process repeated.

In order to read the calibration current and voltage displacements, as well as the film test values, the negatives were sequentially projected by a photographic enlarger on a white surface. The ripple pattern of the rectified dc power supply required some decision as to how the displacements would be read. In order to avoid the influence of any electronic noise or distortion superimposed on the true signals if peak values were read, it was decided to use a hairline placed on the entire signal trace so that the areas defined by the trace above and below the hairline were made as nearly equal as possible. The displacement from the base line signal was read at the point where the hairline crossed the center vertical grid line of the scope, since this point corresponded to the average playback time for that trace as indicated by the electronic timer. In reality, the hairline represented the time-average voltage or current over one trace sweep period at the playback time indicated by the electronic timer for that particular photograph. The trace sweep period was two seconds of playback time or 0.01 second of run (real) time.

Photographic prints were made of the post experiment film as well as any special photographs taken for that test. The final operations for a given test consisted of a post trial weighing of the film on the Mettler balance, and a thorough microscopic examination of the failed film surface.

Conversion of Photographic Data to Thermal Parameters

The run (real) time corresponding to each data photograph was obtained by dividing the photograph playback time by the ratio of the tape recording speed to playback speed, i.e., 200. The voltage and current calibration scale factors to be applied to the test data were obtained by averaging the respective scale factors from the pre-trial and post-trial calibration trace photographs. The current and voltage displacements read from the data photographs were then multiplied by the appropriate calibration scale factor to convert them to volt and ampere values. The ratio of trace voltage to trace current yielded the total test load resistance for each photograph. Subtraction of the experimental test system power lead resistance of 0.1440 ohm converted the total test load resistance to actual film resistance for each photographic frame.

Using the film resistance thus obtained in each data photograph, the average film temperature was estimated from the film thermometric calibration curve. In addition, the power dissipation within the film for each frame was computed by:

$$Q_f(\text{BTU/hr}) = 3.41\ I_f^{\,2}(\text{amperes}^2)\ R_f(\text{ohms}) \quad . \qquad (1)$$

The power dissipation may, of course, be converted into a characteristic film heat flux by dividing Q_f by the film surface area between the electrical contact blades. With this simple procedure, the set of photographic traces were converted to the average film temperature-time and film power dissipation-time histories.

The reduction procedure was very satisfactory except at low power, i.e., near zero time, where the temperature data were often quite scattered.

The scatter was probably a result of reading errors in obtaining the voltage and current displacements. The magnitude of the reading error was constant regardless of the magnitude of the displacement being measured. This resulted in large percentage errors for the small displacement values, and even larger percentage errors in the ratio of these small displacements required for the film resistance-film temperature calculation near the beginning of each test.

CHAPTER IV

THE EFFECT OF THICKNESS, TEMPERATURE, AND TEMPERATURE CYCLING ON THIN METAL FILM ELECTRICAL RESISTANCE

Background

Before any conclusions as to the intrinsic limitations and usefulness of thin film resistance heating elements for transient high heat flux investigations could be attempted, it was thought that the stability and survival of such elements under external cyclic heating should first be examined. In addition, there was an obvious need to ascertain and report any effects that film thickness might have on electrical resistance or its temperature dependence. Consequently, this chapter will first present the results of a specially designed, cyclic high temperature resistance stability test conducted on one typical film each of the three metals utilized in this research program. It will also present a parametric correlation of the effects that film thickness had on both film resistance and the resistance-temperature relations for each film metal. These correlations were obtained by plotting the appropriate data from thermal test films, resistance stability films, and from films that were plated but rejected for thermal testing for one reason or another at a later stage in their processing.

Although similar data abounded in the literature, the application to or comparison with this study was limited due to system dissimilarities, to different orientation or emphasis, or to the often conflicting nature and interpretation of the data. Typical of the more applicable data avail-

able are the works of Belser, et al. (13) and (15), Winding, et al. (2), and Holland (7). Because of the rather specific preparation conditions and techniques utilized in this work, plus the uniquely large size and intended use for the films considered herein, the data presented in this chapter constitute a necessary supplement to the overall research program and final film performance evaluation.

Thin Film Resistance Stability Under External Cyclic Heating in Vacuo

The experiment now described was designed and performed to provide the answers to four basic questions concerning the stability of the characteristic film resistance-temperature relationship for each of the three metals tested, when the films were subjected to vigorous, externally heated thermal cycling. The questions posed were: (1) Are the temperature-resistance relationships for thin metal films sufficiently stable under cyclic operation, even over limited and well defined temperature ranges, to permit their use as continuous monitoring "area" resistance thermometers? (2) If the temperature is cycled in excess of the previous greatest temperature, are all previous temperature-resistance calibration data invalidated? (3) Is there anything extraordinary about the resistance-temperature plot when the temperature exceeds the lowest recrystallization temperature of the bulk metal? (4) Can either complete film failure or surface changes similar to those noted in the thermal test films be produced by slowly varying, long exposure, high temperature, external cyclic heating of thin metal films?

Experimental Procedure

One typical film each of copper, nickel, and aluminum were prepared as described in Chapter III. The plating conditions and resulting film characteristics are summarized in Table 2. Each film was carefully examined under the Watson-Barnet microscope for surface flaws and irregularities prior to calibration. These examinations indicated that the films were of the same quality as the thermal test specimens. In each case a few surface flaws were noted and occasionally a relatively large reflecting region of grain-like appearance would be visible. Following microscopic examination, each film was installed in the vacuum calibration system and the calibration cycles conducted according to the procedure outlined in Chapter III. The actual resistance-temperature curves obtained for copper, nickel, and aluminum are shown in Figures 10, 11, and 12, respectively. Photographs of the post-test films are presented in Figure 13.

Discussion of Stability Results

Study of Figures 10 through 13 provided the answers to the four questions posed. First, it was obvious that repeated thermal cycling to temperatures less than or equal to the plating (or previous maximum) temperature produced no visible change in the temperature-resistance relationship for any of the three metals. It was further noted that the characteristic thermometric relation was almost linear for aluminum and copper (possessing a very slight upward concavity), whereas, the nickel curve was somewhat "S"-shaped possessing an inflection point near 650°F. Such observation and statements constitute an affirmative answer to the first question posed, at least over the temperature range, room-to-plating

Table 2. Stability Test Film Characteristics Summary

Film Physical Property or Plating Parameter (units)	Film Metal		
	Copper	Nickel	Aluminum
Plating Pressure (mm Hg)	1×10^{-5}	8×10^{-6}	8×10^{-6}
Plating Substrate Temperature (^{o}F)	450	700	260
Weight Average Film Thickness (A^{o})	3140	1365	1875
Maximum Calibration Temperature (^{o}F)	1270	1275	890
Calibration Pressure Range (mm Hg)	$(0.2\text{-}7) \times 10^{-4}$	$(0.05\text{-}5) \times 10^{-4}$	$(0.2\text{-}4) \times 10^{-4}$
Room Temperature Film Resistivity (ohm-cm)	1.98×10^{-6}	1.09×10^{-5}	2.90×10^{-6}
Ratio of Film to Bulk Metal Resistivity	1.15	1.40	1.02
Average Film Temperature Coefficient of Resistance ($1/^{o}F$)	1.84×10^{-3}	3.83×10^{-3}	1.99×10^{-3}
Ratio of Film to Bulk Metal Temperature Coefficient	0.86	1.15	0.92

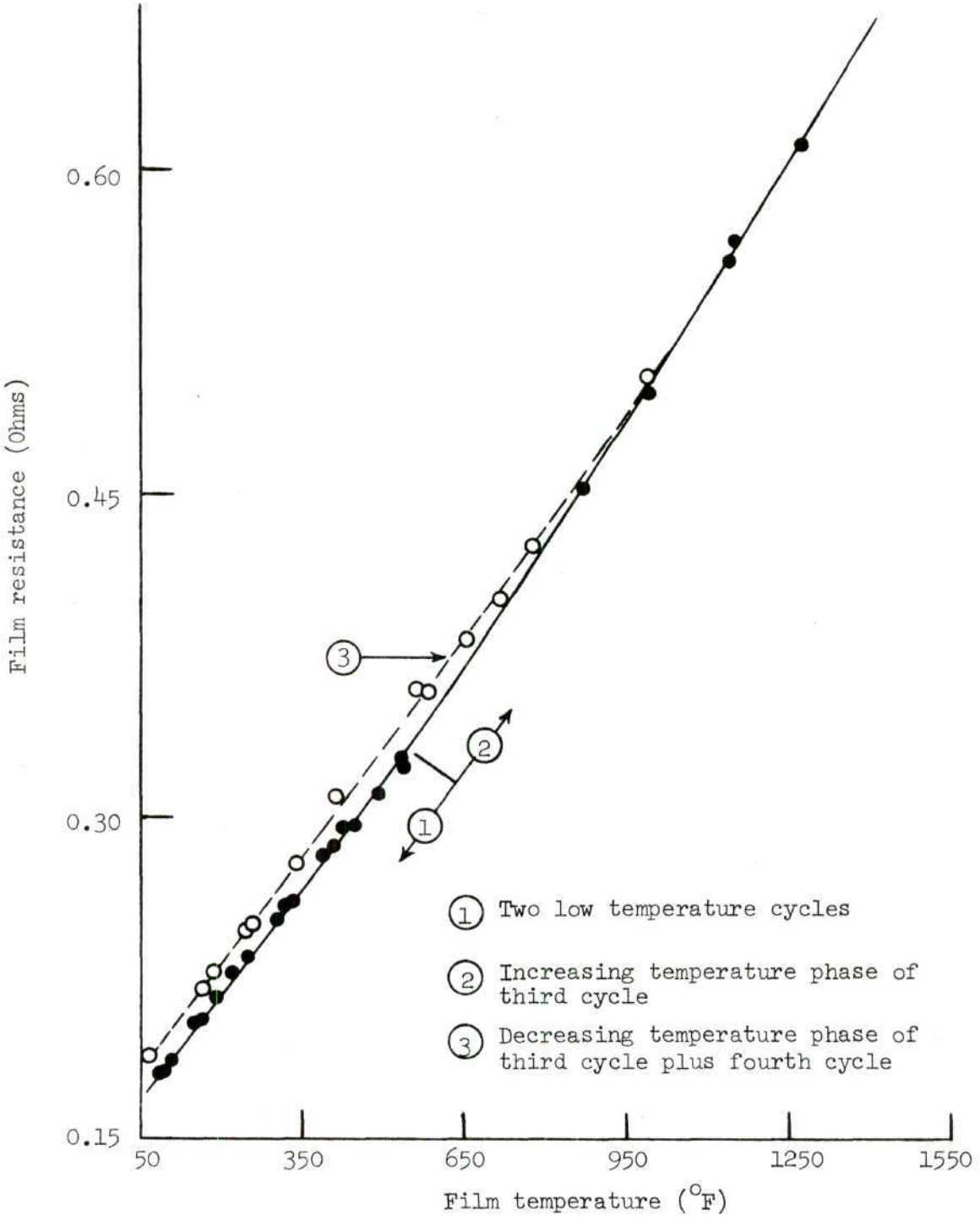

Figure 10. Cyclic Resistance Stability for Copper Films

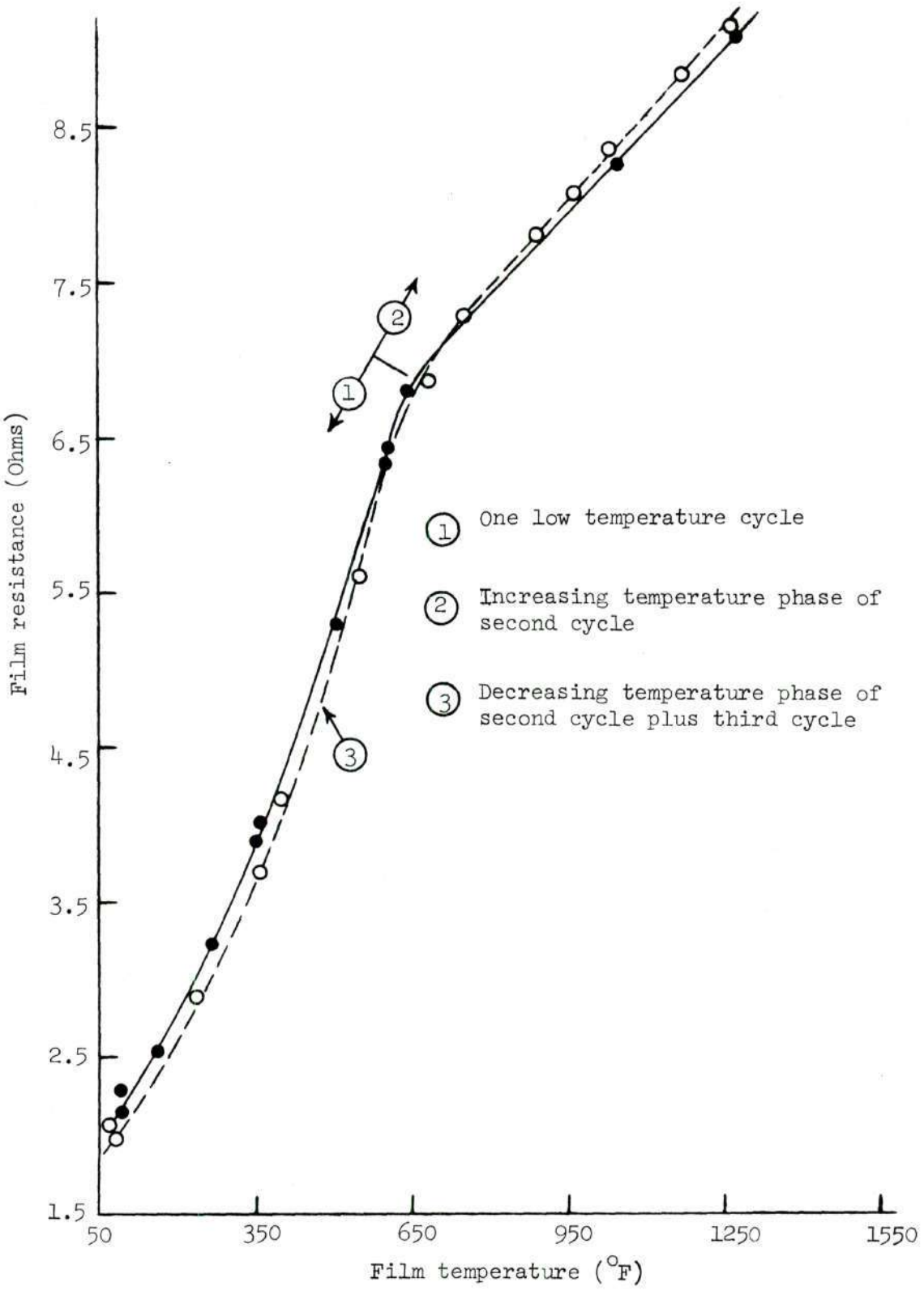

Figure 11. Cyclic Resistance Stability for Nickel Films

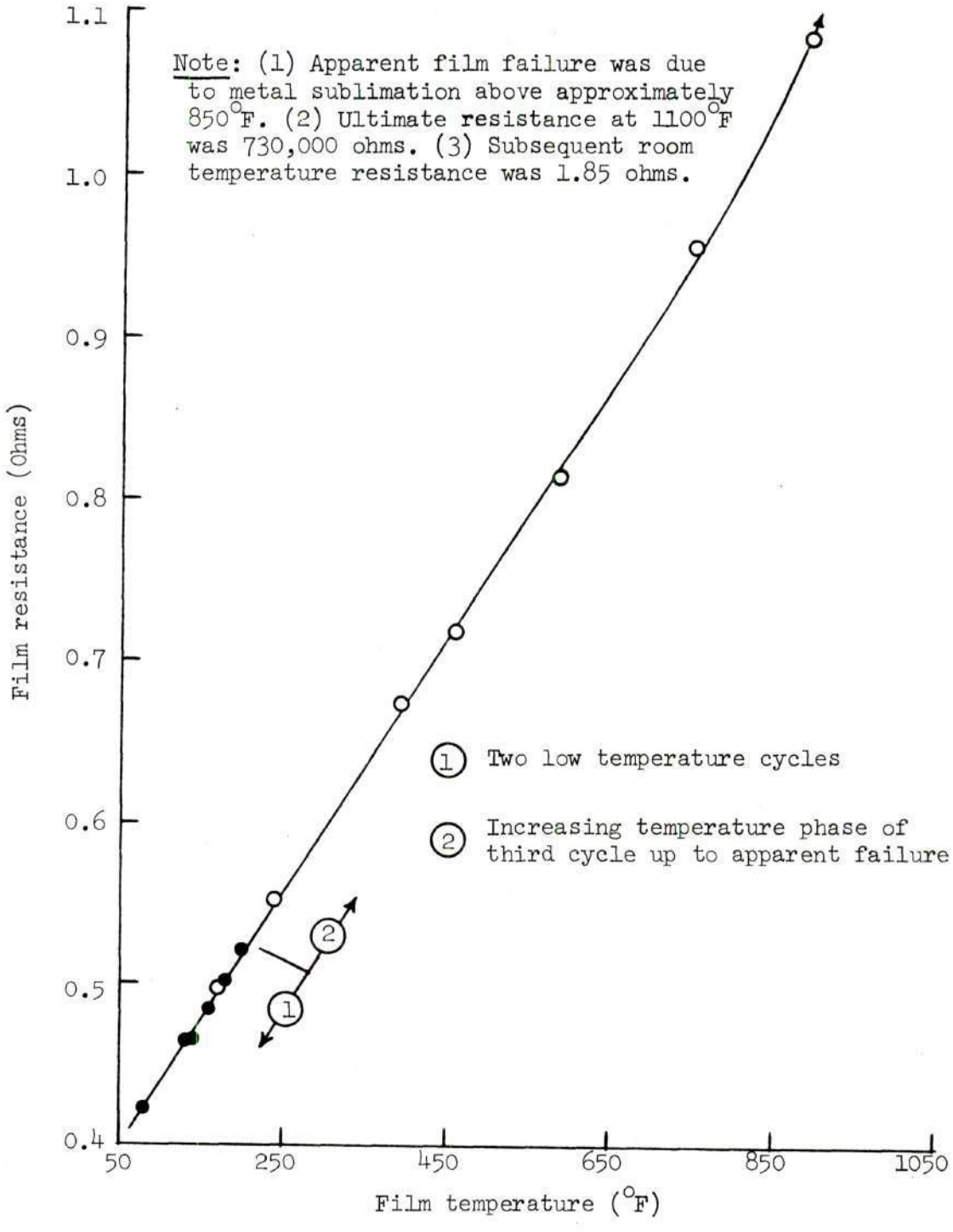

Figure 12. Cyclic Resistance Stability for Aluminum Films

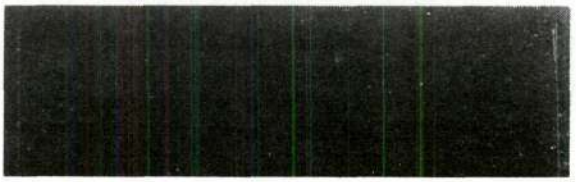

Copper Film

Nickel Film

Aluminum Film

Figure 13. Post-Test Appearance of Cyclic High Temperature Stability Films

or other maximum temperature for which calibration was established. Indeed, any shift in the resistance-temperature plot between cycles for this temperature range was considered insignificant compared to the errors involved in the data collection. These errors were estimated to be a temperature spread of ± 2 per cent about the temperature indicated for any given resistance value.

When the temperature was raised on any given cycle to a level surpassing the greatest previous temperature in the film's history, some hysteresis effect was observed on the down path of that cycle. For copper films the apparent resistance corresponding to a given temperature increased slightly on the down path as compared to the old curve (see dotted line on Figure 10). This down path became the new temperature-resistance curve for subsequent thermal cycles as verified for copper in Figure 10. The hysteresis effect in nickel is illustrated by the dotted curve of Figure 11. The hysteresis amounted to a slight counterclockwise pivoting of the original curve about its inflection zone. The aluminum hysteresis was not obtained due to the sublimation failure. Subsequent aluminum calibration data indicated that aluminum behaves similar to copper, except that the hysteresis curve lies slightly below the original curve rather than above, as in the case of copper. Although hysteresis did occur and must be taken into account in very accurate thermometry applications, three observations permitted the second question posed to be answered negatively. First, the magnitude of the shift in the temperature-resistance curves was seen to be at most 20-30^{o}F at any fixed resistance value, even for the large increase in maximum temperatures between successive cycles illustrated in Figures 10 and 11. Secondly, the shifted curves paralleled closely the

original curves, that is to say, hysteresis shift did not alter the intrinsic shape of the temperature-resistance plot. Thirdly, once the new curve had been established, it became fixed until the new greatest temperature was surpassed. These observations not only provided a basis for a negative answer to question no. 2 but also provided a basis for estimating the magnitude of the hysteresis shift in any given set of cylic conditions as well as a basis for extrapolation of the resistance-temperature plots into "overheated" (uncalibrated) ranges of operation.

Within the limitations of the sensitivity of the equipment and procedure used in this study, nothing extraordinary was observed in the temperature-resistance curves for any of the three metals in the region of the lowest recrystallization temperature of the bulk metal. The lowest recrystallization temperatures for bulk copper, nickel, and aluminum according to Samans (18) are 390°F, 1110°F, and 300°F, respectively. It should be noted that these temperatures were exceeded on at least one cycle for each of the metals tested in this substudy.

As to the question of film failure or severe surface damage, neither the nickel nor copper film showed any evidence of failure or imminent failure in these tests, even when subjected to temperatures approaching 1300°F for periods in excess of one hour under a vacuum of 5×10^{-4} mm of Hg. The aluminum film indicated an apparent failure (resistance becoming very large) when the temperature exceeded 900°F under a vacuum of 5×10^{-5} mm of Hg. Subsequent examination of the aluminum film, however, indicated that the apparent failure was caused by severe sublimation metal loss in the regions around the contact blades, rather than through any process similar to that observed during the thermal testing (see Figure 13).

Following these tests, the films were once again examined under the microscope. In each case the film was no longer the mirror-like reflector of oblique light that it was prior to calibration. Instead, each film appeared to be cloudy, indicating that the post-test surface consisted of a large number of randomly oriented reflecting centers. Under higher magnification, the small, uniform grain structure of each film surface became visibly clear. The few large reflection centers which had been observed prior to calibration now appeared subdivided into grains equal in size with those of the remainder of the film surface, the outlines of the original centers remaining clearly visible.

This visual evidence of film surface reconstitution when the bulk recrystallization temperature had been exceeded in each case, strongly suggested that recrystallization of the film surface did indeed occur under conditions and in a manner similar to that of the bulk metal. Recrystallization is known to be a complex rate process with such factors as impurities, available recrystallization sites (a strong function of previous metal strain), soaking time at temperatures above the recrystallization temperature, and the actual amount of temperature increase over the recrystallization temperature playing a role in the rate and extent to which recrystallization takes place. The fact that copper, which was plated at a temperature above its recrystallization temperature, was not observed during precalibration examination to be recrystallized could be explained in terms of the very short soaking time above 390°F, and the small overheat of 60°F available for initiation of the process.

One additional fact supported the conclusion of thin film recrystallization during these tests. The copper and aluminum films both experienced

a much greater overheat of their recrystallization temperatures than the overheat experienced by the nickel film. In addition, the soaking times at temperatures above the recrystallization temperatures for copper and aluminum were much greater than that of the nickel film. It was known from the literature, Samans (18), that following recrystallization, grain growth would occur either if the sample were heated substantially above the recrystallization temperature or soaked for extended periods of time just above the recrystallization temperature. Therefore, if the surface changes described previously were in actuality a result of film recrystallization, then the post calibration grain size of both the copper and aluminum films would be expected to be larger than that of the nickel film. Such was indeed observed to be the case upon microscopic comparison.

From the data gathered in this investigation, the significant results and conclusions may be summarized by stating that: (1) Under a chemically inert environment approximating that of the vacuum used in this study, copper, nickel, and aluminum films possess usefully stable resistance-temperature properties when subjected to externally heated temperature cycles over the range (70-1300)$^{\circ}$F for copper or nickel, and (70-750)$^{\circ}$F for aluminum. (2) Small, predictable hysteresis shift occurs whenever the previous history maximum temperature is exceeded on a given cycle, the shifted curve becoming the new, stable resistance-temperature relation. (3) For the above temperature ranges, neither film failure nor striation surface effects similar to those noted on the fired thermal test films were observed, even though these temperatures exceeded greatly in some cases the measured maximum temperatures of the thermal test specimens. (4) The film resistance stability and survivalability appeared to be unaffected as

the temperature was raised above the bulk metal recrystallization point, even though the evidence indicated strongly that each film underwent a complete surface rearrangement not unlike bulk metal recrystallization during these tests.

Film Resistance and Resistivity Dependence on Film Thickness

Figures 14, 15, and 16 present for copper, nickel, and aluminum films, respectively, the room temperature film resistance and film resistivity as functions of the weight average film thickness. From these figures it was observed that for each metal there appeared to be an average thickness range below which the film resistance increased rapidly with decreasing thickness, whereas increases in thickness above that range produced only relatively small decreases in film resistance. These approximate thickness ranges were (3500-4000)Å for copper, (3000-3500)Å for nickel, and (1850-2350)Å for aluminum.

The figures also revealed that the resistivity curves for these three metals tend to be "U"-shaped. The bottom of the "U" for each metal lies above the bulk resistivity with the ratio of film-to-bulk resistivity at the point of closest approach being 1.11 for copper, 1.10 for nickel, and 1.01 for aluminum. The approximate thickness for each film metal corresponding to the point of closest approach to the bulk resistivity was 2600 Å for copper, 2500 Å for nickel, and 2100 Å for aluminum. The range of film thickness for each metal constituting the base of the "U", i.e., the range of thickness where the resistivity was relatively independent of thickness and nearest the bulk value, was observed to be (2300-3100)Å for copper, (1100-3400)Å for nickel, and (1800-3000)Å for aluminum.

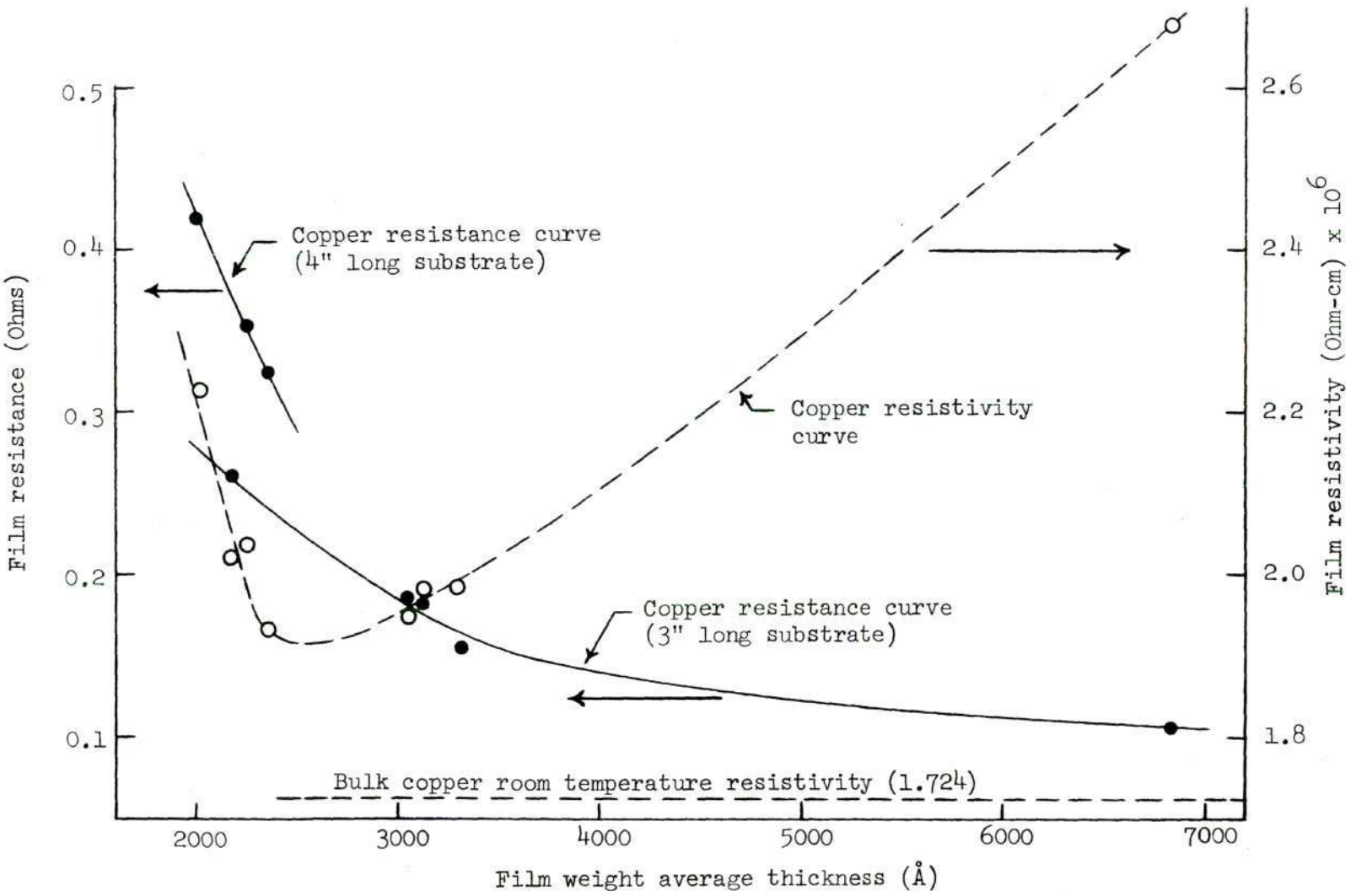

Figure 14. Copper Film Room Temperature Resistance and Resistivity Thickness Dependence

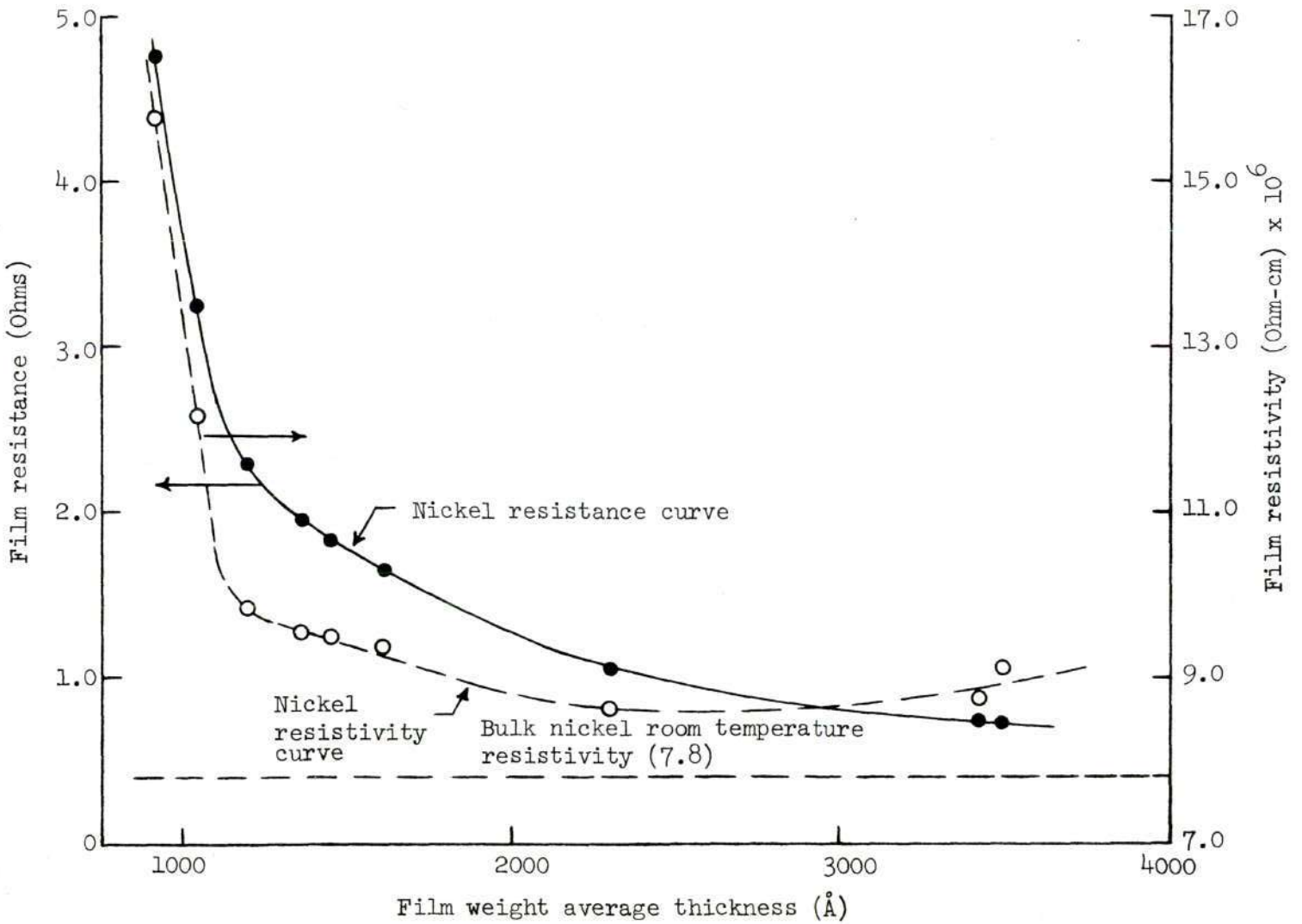

Figure 15. Nickel Film Room Temperature Resistance and Resistivity Thickness Dependence

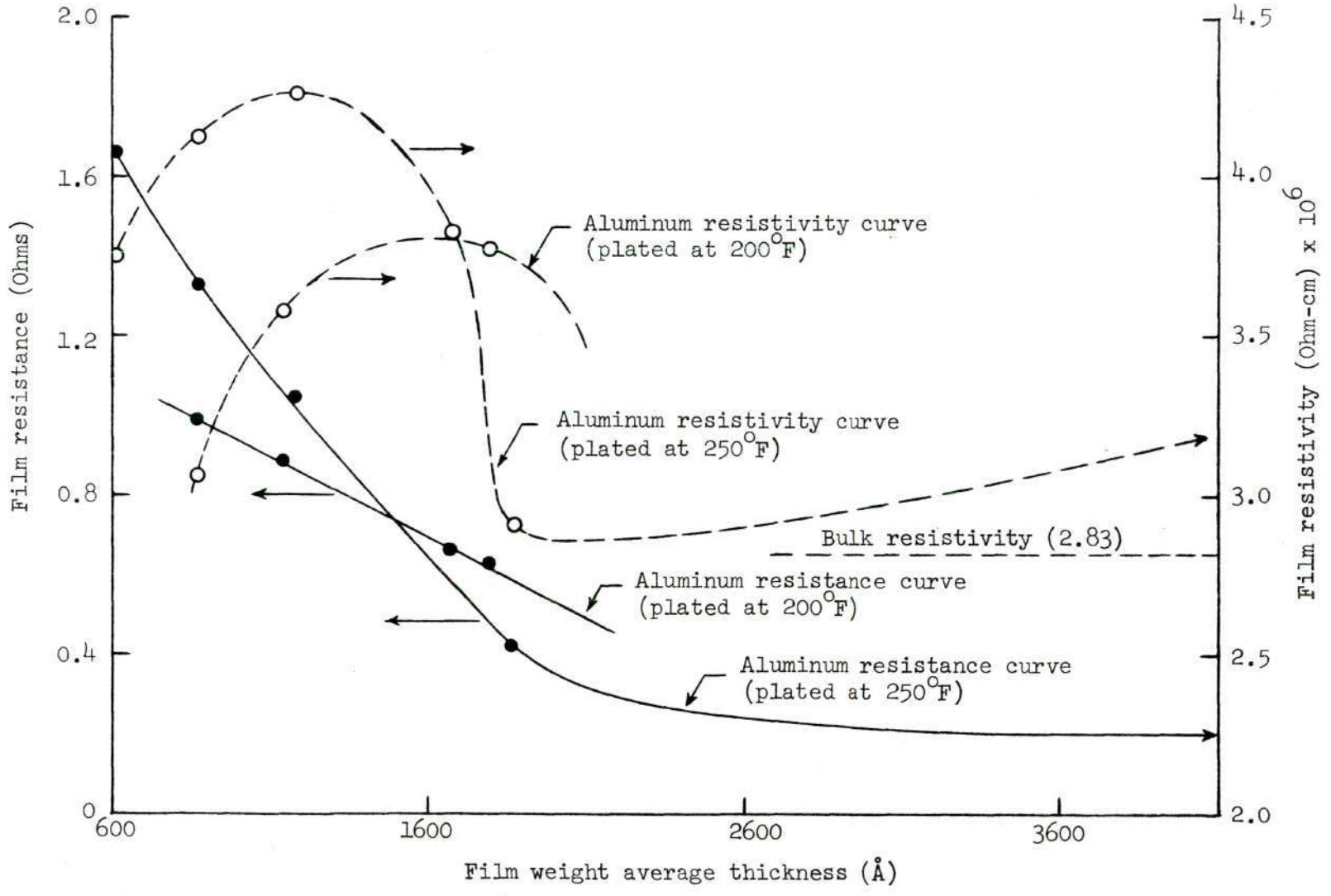

Figure 16. Aluminum Film Room Temperature Resistance and Resistivity Thickness Dependence

Examination of the data of Figure 15 revealed a plating temperature dependence of both the resistance and resistivity for aluminum films below a thickness of 1600 Å. In this low thickness region both the film resistance and resistivity for a given thickness were greater at a plating temperature of approximately 250°F than at 200°F. In addition, it may be observed that aluminum films plated at either temperature exhibit a relative maximum in the resistivity curve before degeneration into the "U" shape previously noted for all three metals. The observed aluminum resistivity behavior may be analyzed in terms of the nature of the vapor deposition process.

Possibly for very thin films, sufficient energy was available at either plating temperature to permit the immediate removal, by diffusion to the film surface, of a significant fraction of the vapor impurities, vacancies, and other lattice imperfections created by the violent shock of deposition. Such a significant removal would result in a relatively small film resistivity. As the thickness was slightly increased, the available energy may have been insufficient to permit the diffusion of as great a fraction of the lattice impurities and imperfections over the increased distances to the film surface, thus resulting in an increased resistivity. As the thickness was further increased, the initially arriving metal layers could have acted like a getter to permit the subsequent metal build-up to be more bulk-like in its lattice formation. Consequently, the more highly stressed, high resistivity zone tended to become restricted to the film-substrate boundary, and its relative influence on the overall resistivity reduced with increasing thickness. Such a concept of the film behavior during continuous vacuum vapor deposition adequately explains the observed

progressive attainment of a relative maximum, followed by a decrease and subsequent leveling off of the resistivity curve with increasing thickness. Similar logic, of course, applies to the copper and nickel films, and serves to explain the left leg and bottom region of their "U"-shaped resistivity curves. Sufficiently thin films of copper and nickel were not considered to obtain their relative maximum peaks in the low thickness region, if indeed they exist. Over the range of plating temperatures employed for copper and nickel films, no temperature dependence was observed for either resistance or resistivity for these metals.

The logic train just presented leaves unexplained the right leg of the "U"-shaped resistivity curves and the observed plating temperature dependence of aluminum resistivity at small thicknesses. The attempted explanation of the effect of plating temperature on aluminum film resistivity had its foundation in observations described in the literature of the very great tendency for aluminum to oxidize, even under exposure to the very low oxygen concentrations encountered in vacuum deposition. The higher plating temperature would tend to increase the amount of oxidation experienced by the metal during film deposition. For very thin films, the oxide could be formed virtually all the way through the film thickness, resulting in a higher resistivity film than that of the same amount of metal plated on the cooler substrate. As the film thickness was increased, however, oxidation should become more restricted to the substrate (oxidation of initial metal layers) and outer film surfaces (oxidation of the last few metal layers) with a correspondingly reduced influence on overall film resistivity. In addition, the increased mobility of lattice vacancies and imperfections at the higher plating temperature should tend to counter the

effects of increased oxidation on film resistivity. With these counter effects of temperature at play, it was not surprising that both the resistance and resistivity curves for the two plating temperatures converged and possibly crossed as the film thickness was raised from 600 Å to 1600 Å.

The rise in resistivity observed for all three metals at the larger thicknesses, i.e., the right leg of the "U"-shaped resistivity curves, was attributed to the formation of a "laminated" film structure resulting from variations in the deposition rate invariably experienced during production of the thicker films. It will be recalled that in the discussion of Chapter III concerning the deposition process, once the film metal was melted on the plating filament, the power was increased as rapidly as possible without throwing molten metal from the source beads until deposition was complete. For a relatively small number of source beads, i.e., thinner films, high, constant deposition rates could easily be maintained and the thickness-resistivity discussion of the preceding paragraphs was valid. However, as the number of source beads grew, the initial power surge would not always completely vaporize all of the source beads, and often the deposition rate would fall sharply before a second power surge could be applied to finish the deposition. This dwell in deposition rate for the thicker films would tend to nullify the gettering action of the initial deposit. The second deposition surge would then experience plating conditions similar to the initial conditions, with the result that a high stress, large resistivity zone or layer was introduced into the middle of the thicker films. A thicker film would then possess a resistivity higher than that of a somewhat thinner film that was deposited in one short, strong burst.

Film Temperature Coefficient of Resistance Dependence on Film Thickness

Figure 17 presents a plot of the film temperature coefficient of resistance for each metal as a function of film thickness. In the case of aluminum and copper, which have very nearly linear temperature-resistance relationships, the temperature coefficient values plotted represent true room temperature coefficients. The values plotted for nickel are larger than the true room temperature coefficient because the slope of the temperature resistance plot utilized was an average value over the calibration temperature range. In each case the average slope was greater than the room temperature slope due to the "S" shape of the nickel temperature-resistance relation.

From Figure 17 it was observed that the copper coefficient was independent of thickness with the value being slightly less than the bulk value. For aluminum the coefficient appeared to increase slightly with increasing thickness, approaching the bulk value from below. The nickel coefficient appeared to increase slightly with increasing thickness with the values lying above the bulk value. The ratio of copper film to bulk coefficient was 0.88. The ratio of aluminum film to bulk coefficient increased from 0.70 to 0.82 as the thickness increased from 500 Å to 2000 Å. The nickel film to bulk coefficient ratio increased from 1.0 to 1.33 as the thickness increased from 500 Å to 3500 Å. As a general remark, it may be concluded that over the range of film thicknesses involved for each metal in this work, the film temperature coefficients were relatively independent of film thickness, and were approximately equal to the bulk metal values.

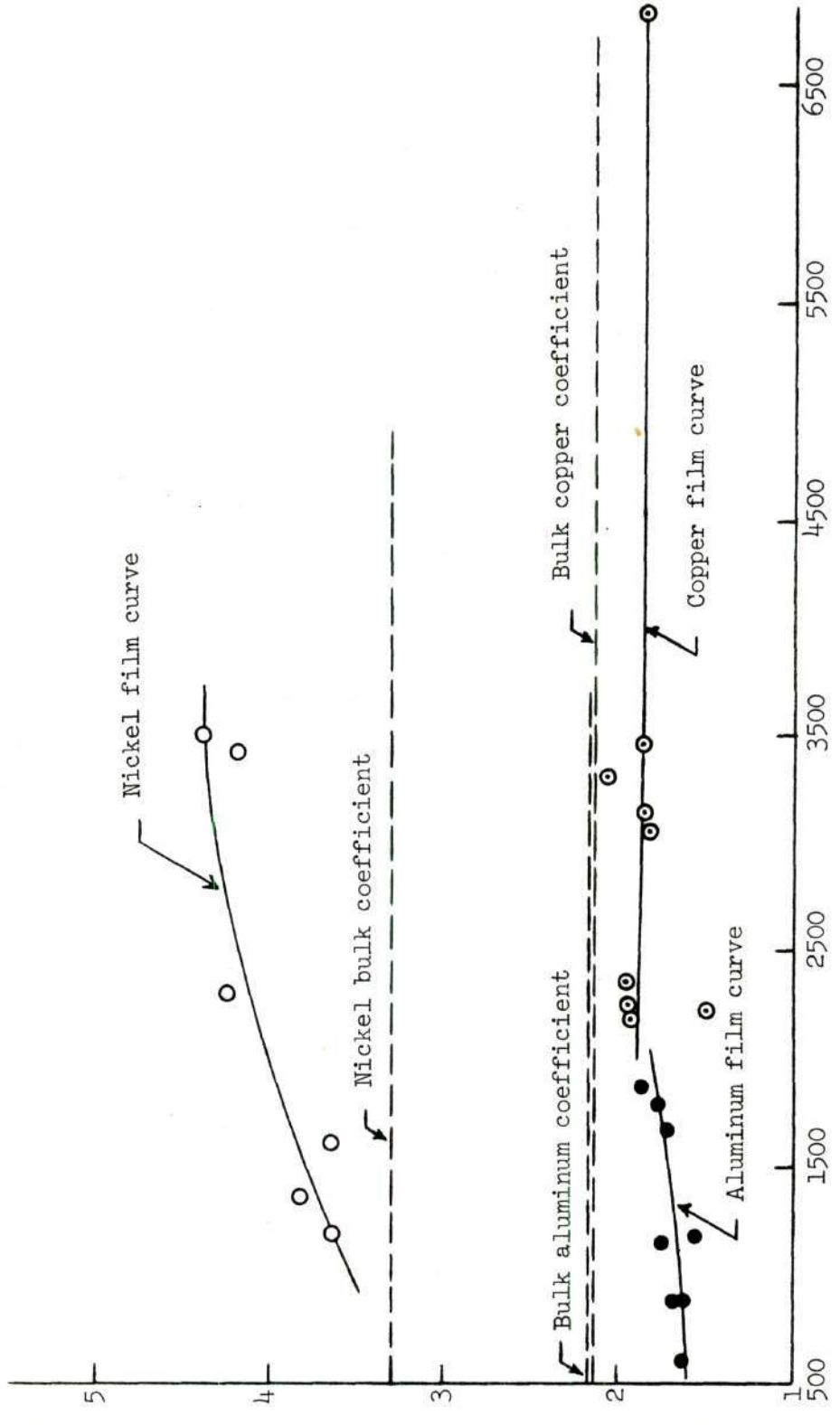

Figure 17. Calibration Average Temperature Coefficient of Resistance Versus Average Thickness for Copper, Nickel, and Aluminum Films

CHAPTER V

FILM UNIFORMITY AND THICKNESS DISTRIBUTION

Background

In the thermal studies described in previous chapters of this work, as well as those of Bomar (5), Fleming (3), and Winding, et al. (1) and (2), the assumption of a unique relation between temperature and film resistance must be made in order that "film heat flux" or "film temperature" as a function of time may be calculated from the measured electrical parameters. Bomar (5) briefly described a technique which was developed in conjunction with this investigator to determine the film thickness distribution of thin metal films, presenting his data for nickel. In his work, however, Bomar used these data only as a semi-quantitative backup for his qualitative assessment of non-uniformity effects on film behavior. Since a truly quantitative interpretation of these data was essential to the film behavior modeling presented later in this work, and since in addition, the technique was applied to copper as well as to nickel films, a complete description of the technique and its results are presented in this chapter.

General

The technique is basically an iterative coupling of microgravimetric analysis and X-ray flourescence. It is based on the idea that if the metal film is thin enough so that the incoming source X-ray and emerging emission X-ray beams are neglibly attenuated by the film, then the emission beam intensity is a direct measure of the amount of metal on the region being

scanned. For this particular study, the technique was considered superior to more classical methods such as interferometry, since the test is non-destructive, avoids the edge preparation problem, but most importantly provides average thicknesses over significant areas which are at the same time small relative to the total film surface. The use of X-ray fluorescence in film thickness measurement was shown to be practical in unpublished work by Hearn (19).

Sample Preparation

Each substrate used in this investigation was cut into six approximately equal segments ($\frac{1}{2}$ x 1 inch). Each segment was marked by a scratch code on its under side, indicating the slide to which it belonged as well as its position within the reassembled slide. The segments were then cleaned by the procedure outlined in Chapter III, and weighed to the nearest 0.01 milligram on a Mettler, Type B-6, Gram-atic balance. The plating surface area was computed for each segment by multiplying the assembled substrate plating area (1 x 3 inches) by the ratio of the segment weight to the sum of the segment weights.

The substrate was assembled on the substrate heater platform and plated as described for the appropriate metal in Chapter III. It should be pointed out at this point that aluminum films are not directly considered in this investigation. The aluminum emission X-ray is so soft that beam attenuation by air at one atmosphere dictated the use of vacuum fluorescence, whereas the vacuum fluorescence system on the available Siemens Crystalloflux IV unit was considered unreliable due to persistent, intermittant, and unresolvable leakage. It was thought that no loss in

completeness was incurred, however, since copper and aluminum were both plated from a wire-wrapped filament, presenting no particular difficulty in regard to filament alloying or fluxing. The results for copper should be directly applicable to the aluminum films.

After plating, the segments were again weighed on the Mettler balance and the weight average film thickness for each segment calculated. In this calculation the segment surface area, as obtained above, and the density of the bulk metal were used.

X-Ray Fluorescence Analysis

Two special sample holders for the Siemens Crystalloflux IV were fabricated, one low in copper, the other low in nickel content. The apertures in the holders were cut approximately 1/4 x 3/8 inch, thereby allowing three exposures to be made on each segment. The exposure pattern is illustrated in Figure 18.

Source X-rays were provided by a tungsten tube operated at 50 kilovolts and 14 milliamperes for all exposures. The emission X-rays were diffracted through a standard lithium flouride diffraction crystal and detected by a proportional counter, both of which were mounted on the Siemens goniometer. The proportional counter was operated on its voltage plateau with the proper energy discrimination band to insure that only those X-rays of the desired energy, namely, the K-alpha emission for each metal, were counted. The output of the counter was recorded on a strip chart. For maximum sensitivity, the angle corresponding to that of greatest K-alpha intensity was chosen as the analysis peak for each metal. Using a series of early test segments of the appropriate film thickness,

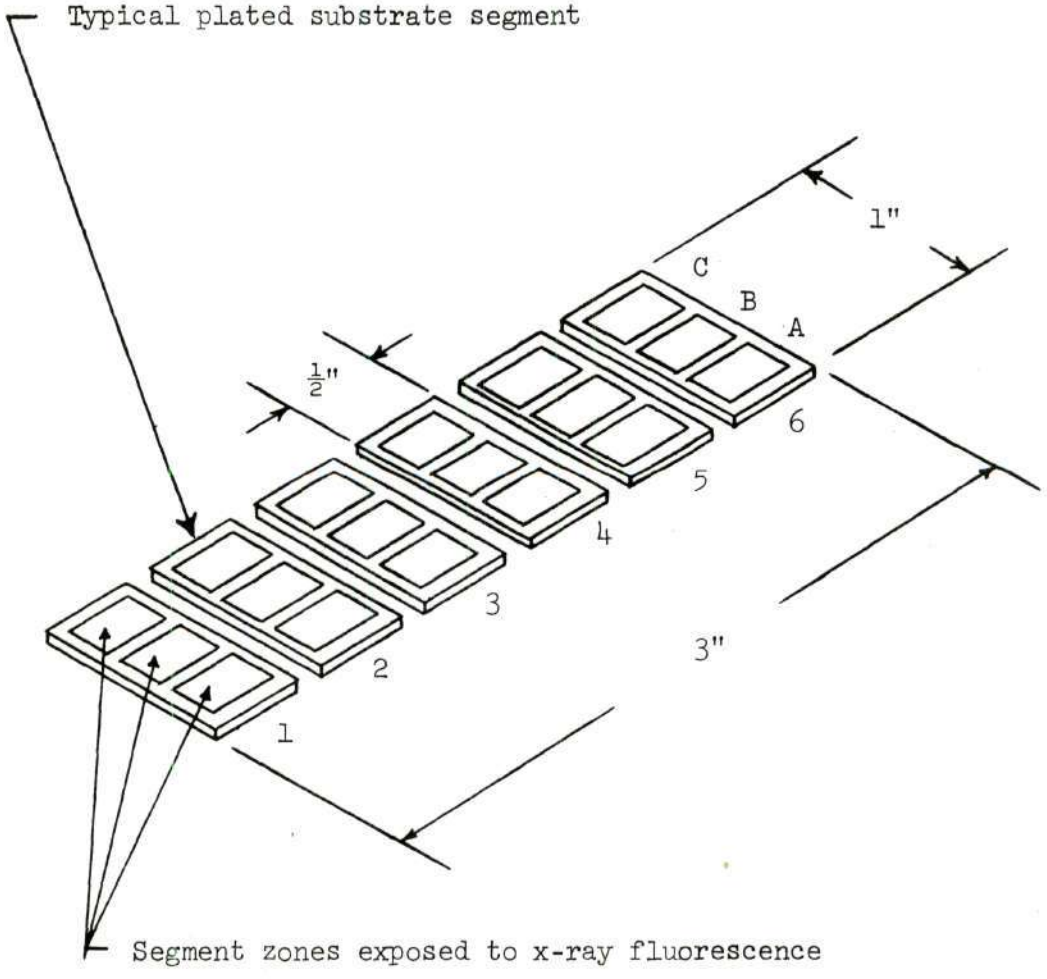

Figure 18. Film Thickness Investigation Substrate Division, Marking, and X-Ray Fluorescence Exposure Pattern

such operating conditions for the Siemens unit as scan rate, intensity scale factor, and chart speed were established and standardized for each metal.

During these early fluorescence tests it was observed that even while using constant source and standardized unit operating conditions, considerable differences in peak height and area might be occasionally realized from the same segment from exposure to exposure, particularly if the exposures were separated by a sizeable time interval. Some of this drift behavior could be attributed to the statistical nature of the emission and counting processes, but the majority of this drift was explained in terms of small perturbations in the power supply to the source tube, thereby producing perturbations in the source X-ray, and ultimately in the emission X-ray intensities. Obviously, if this drift behavior could not either be eliminated or normalized, the use of X-ray fluorescence for a film thickness distribution investigation would be meaningless. After some effort it was concluded that the intrinsic stability of the Siemens unit as installed could not be greatly improved. As a result, a testing procedure was designed to normalize the drift effect and make the fluorescence technique workable.

The testing procedure developed was as follows: (1) The Siemens unit was adjusted to the standard operating conditions appropriate for the metal involved. (2) The unit was turned on and allowed to warm for a minimum of two hours prior to testing. (3) The special holder (low in content of the metal being tested) was placed in the unit and a trace taken as though the holder contained a sample. (4) An infinitely thick (relative to the film) piece of the metal being tested was placed in the holder and

another trace taken. (5) A test segment was then inserted into the holder and three traces across the segment, as indicated in Figure 18, were made as rapidly as possible. (6) Steps 3 and 4 were then repeated. These six steps were repeated for each segment until the complete substrate had been tested. The Siemens unit was left on while the strip chart data were analyzed to see if any of the segment traces should be voided due to drift. This analysis consisted of a simple comparison of the two infinite sample peak areas (corrected in each case by subtraction of the corresponding sample holder peak area) which bracketed each set of segment film traces. It was thought that if these two constant or known thickness trace areas, taken immediately before and after the three film traces for a given segment, were in satisfactory agreement then the probability of drift effects within the three film traces for that segment would be acceptably small. Since the error involved in measuring the film trace areas had been estimated to be approximately 5 per cent in early tests, it was judged that a 5 per cent spread in the corrected infinite sample peak areas bracketing any given segment data was satisfactory with regard to segment drift stability acceptance. Those segments not meeting this criteria were immediately returned to the Siemens unit for retesting. After all the data had met the drift criteria, the X-ray unit was shut down and the remaining peak (trace) areas were determined. All peak areas were determined in this study through the use of a polar planimeter directly on the strip chart plots. Each peak (trace) was remeasured until successive readings agreed to within ± 0.02 square inch.

Having satisfactorily reduced drift effects within the data for each segment, it became necessary to develop a rationale for correlation

of the data from segment to segment. Since the infinite sample peak areas should remain constant for all traces if drift were not a problem, it was decided that a correlation would be attempted using normalized peak areas, that is, the ratio of a given film trace area to that of its own segment infinite sample area. Implicit in this procedure was the assumption that film trace areas were affected to the same relative degree by drift as were the infinite sample areas. Though such an assumption appears plausible, no direct proof to substantiate it can be given.

Therefore, from each film trace area of a given segment, the linear average sample holder trace area for that segment data was subtracted. The adjusted film areas were identified by the symbol A_f. The normalizing area for the segment was then obtained by subtraction of the linear average sample holder trace area for the segment from the linear average infinite sample trace area for the segment. This normalizing area was identified by the symbol A_∞. The three ratios, A_f/A_∞, for the segment were then calculated, and the whole procedure repeated segment by segment until the entire substrate data were normalized.

Weight-Fluorescence Correlation and Thickness Distribution

At this point it became necessary to correlate the weight data with the fluorescence data in order that some useful insight into the distribution of film thickness from zone to zone on the substrate might be obtained. For this correlation, it was hypothesized that the linear average of the three ratios of film trace area to normalizing area (A_f/A_∞) for a given segment could be taken as a measure of the mass average film thickness for that same segment. Consequently, the mass average film thickness for a

given segment was plotted against the average area ratio for that same segment and a weight-fluorescence calibration curve constructed for each metal. The thickness of each zone was then "back" calculated using each individual zone film trace area to normalizing area ratio (A_f/A_∞) in conjunction with the applicable calibration curve. This iterative-type coupling of the average thickness data for each segment with the normalized area ratios from the fluorescence analysis formed the basis of all results presented in this chapter.

Tables 9 through 12 of Appendix I show the raw weight and fluorescence data, plus the fluorescence normalization process for the copper films analyzed. Tables 13 through 17 of the same Appendix present these data for the nickel films. The resultant weight-fluorescence calibration curves for copper and nickel films are presented in Figures 19 and 20. Tables 18 and 19 of Appendix I provide complete summaries of the "back" calculated film thickness distribution for the copper and nickel films, respectively. These data plotted as thickness profiles are presented in Figures 21 through 24. In Figures 21 through 24 the length of each vertical line emanating from the centers of the eighteen zones sampled on each substrate is proportional to the thickness of that zone.

Theoretical Prediction of Thickness Distribution

Due to the somewhat unique experimental technique just presented for thickness distribution measurement, it was decided that a theoretical calculation should be attempted in order to verify the results. The theoretical treatment presented here is based upon the following assumptions and general observations of the plating operation as conducted in

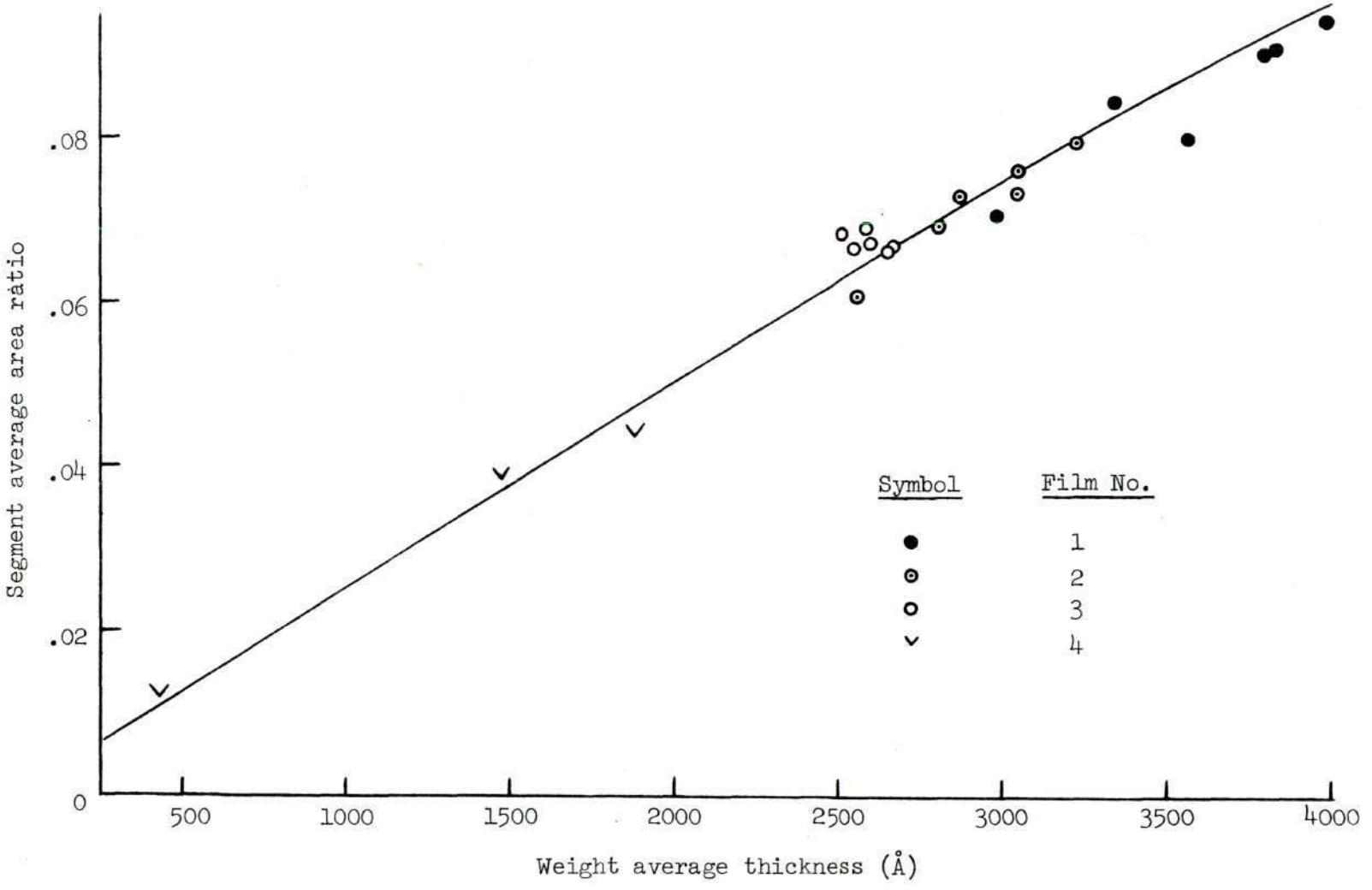

Figure 19. Weight-X-Ray Fluorescence Film Thickness Calibration Curve for Copper

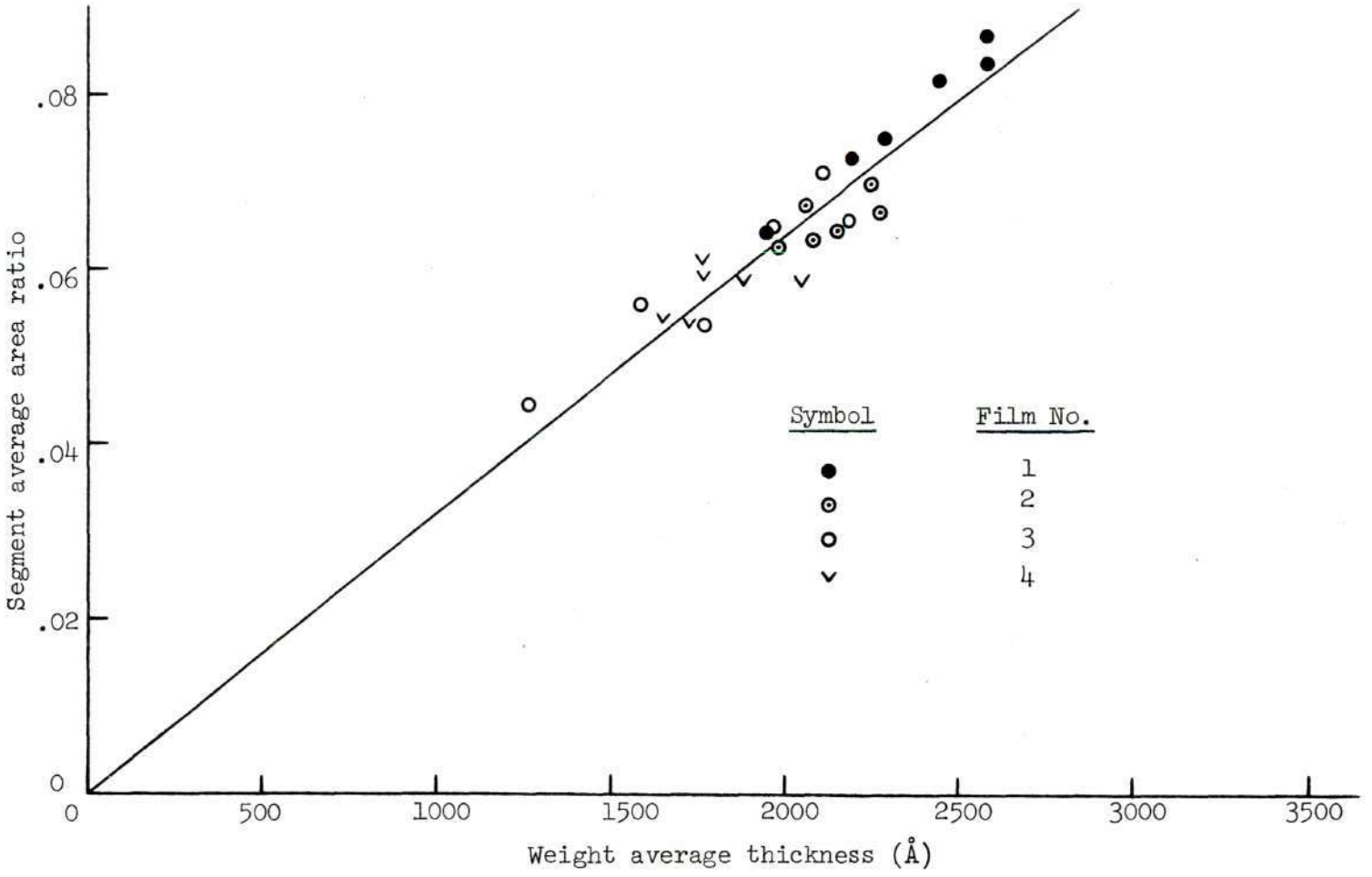

Figure 20. Weight-X-Ray Fluorescence Film Thickness Calibration Curve for Nickel

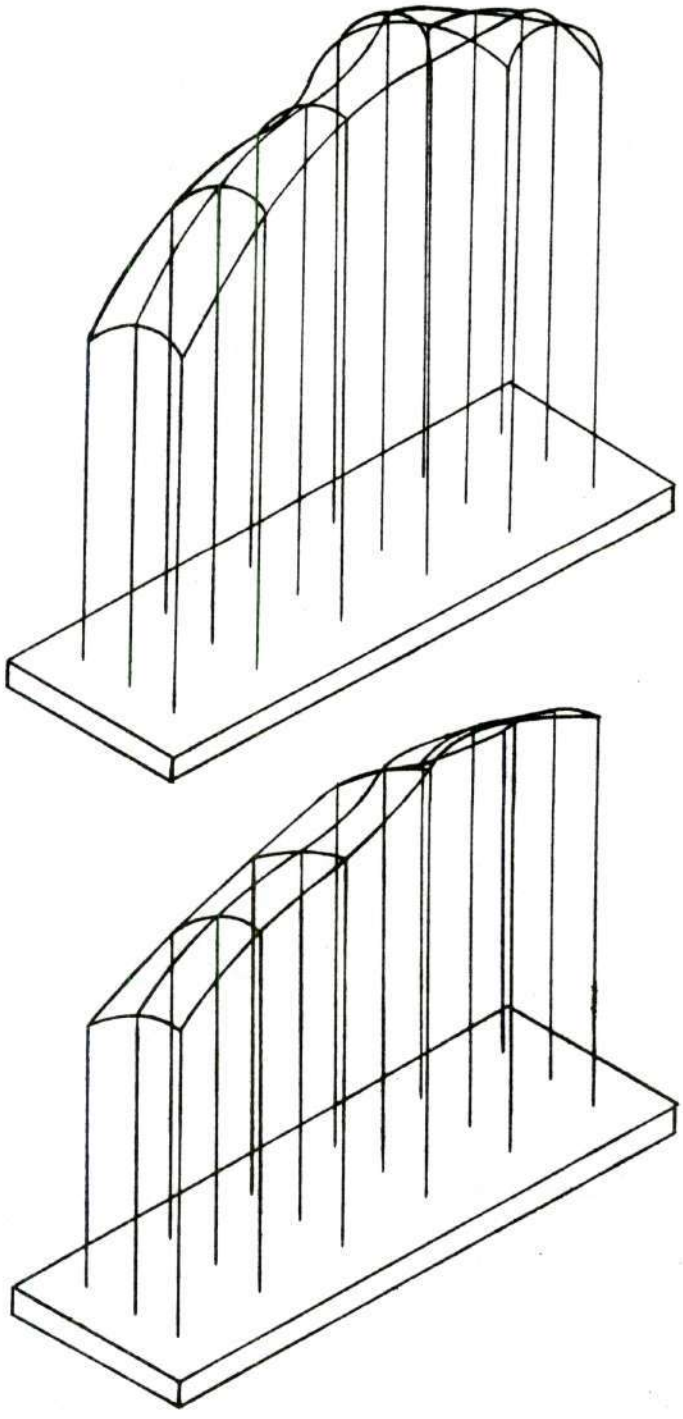

Copper Uniformity
Film No. 1

Copper Uniformity
Film No. 2

Figure 21. Thickness Distribution Profiles for Copper Uniformity Films 1 and 2

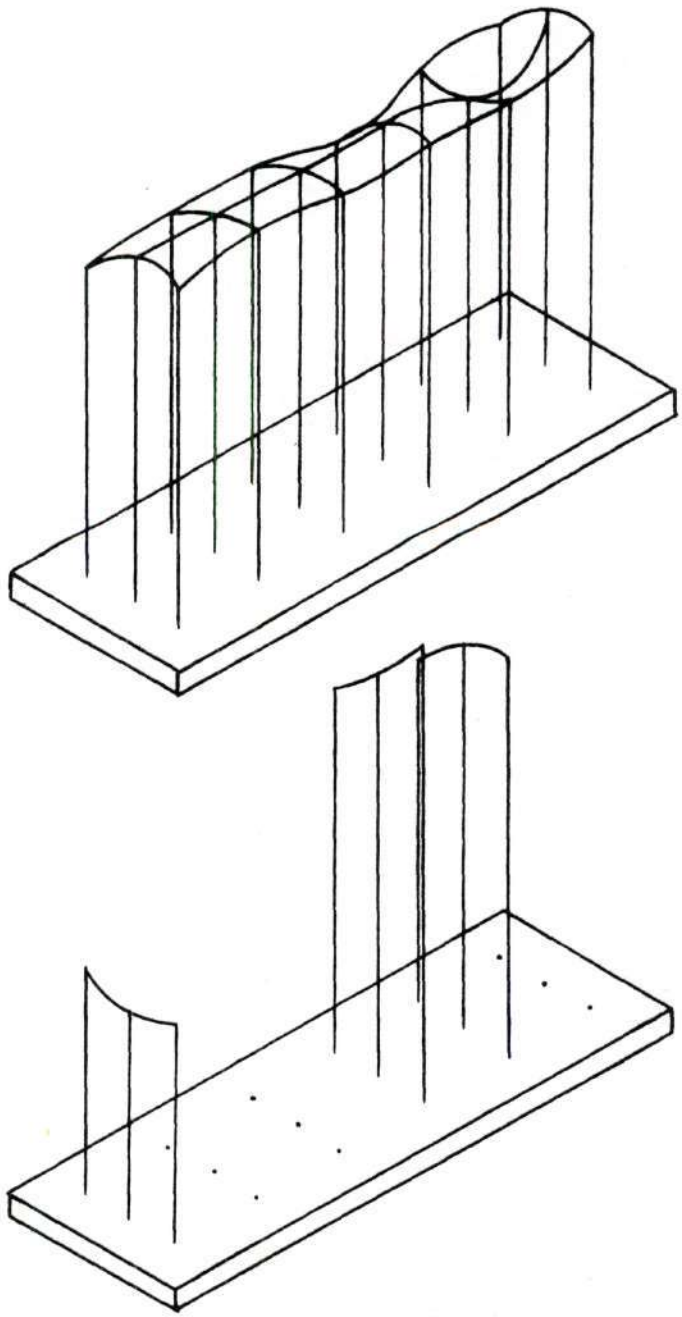

Copper Uniformity
Film No. 3

Copper Uniformity
Film No. 4

Figure 22. Thickness Distribution Profiles for Copper Uniformity Films 3 and 4

Nickel Uniformity
Film No. 1

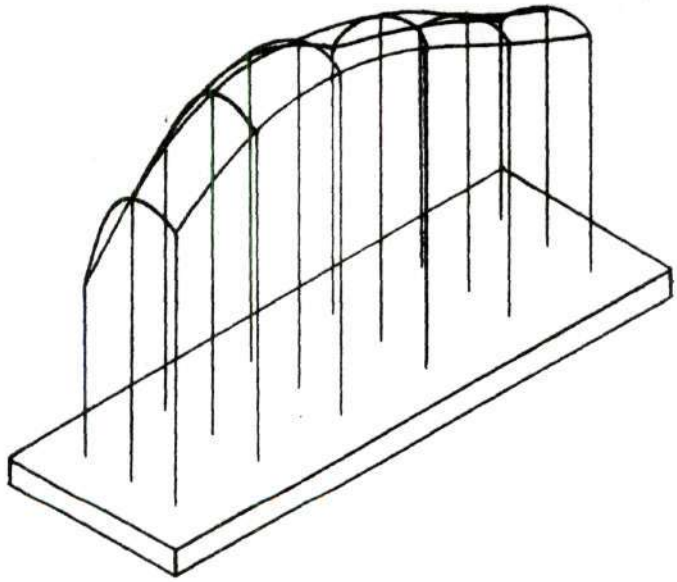

Nickel Uniformity
Film No. 2

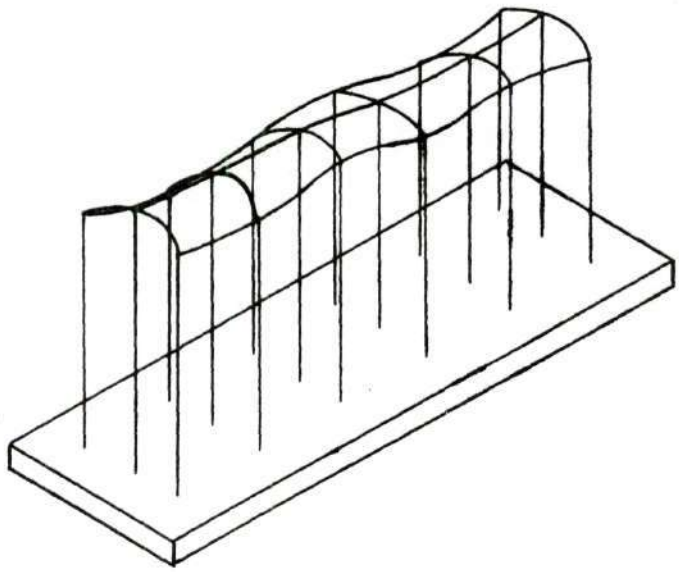

Figure 23. Thickness Distribution Profiles for Nickel Uniformity Films 1 and 2

Nickel Uniformity
Film No. 3

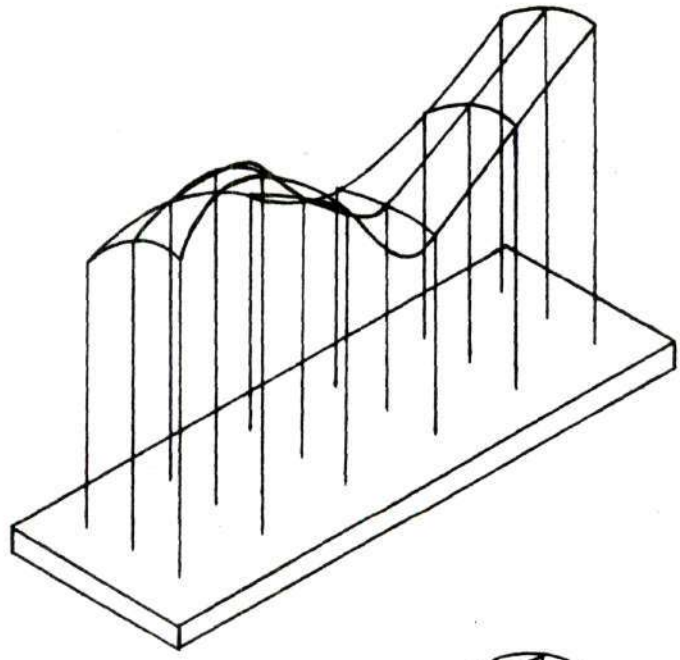

Nickel Uniformity
Film No. 4

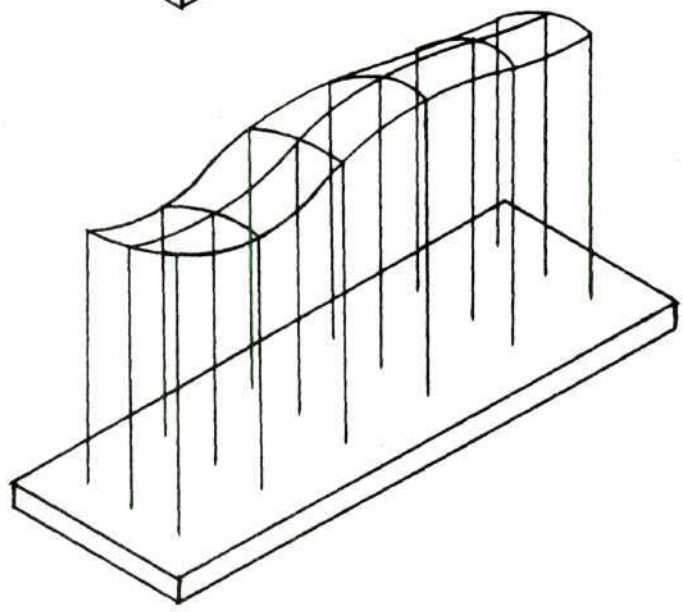

Figure 24. Thickness Distribution Profiles for Nickel Uniformity Films 3 and 4

this work: (1) The bulk of the metal evaporation from the filament occurred not from a line or ribbon geometry, but rather from a series of approximately equal size metal beads fixed along the filament. The beads were formed by the metal surface tension following melting in the early phases of plating. Approximate size equality was verified visually, and by the fact that most of the beads disappeared at about the same instant at the end of the plating process. (2) The number of beads varied from plating to plating with five to eight being the most common. (3) Bead location was found to be slightly dependent upon the filament shape; however, beads invariably were located on the ends of the filament (in the curved regions) and also near the filament center. The latter observation was attributed to the sagging of the filament center due to the thermal expansion of the filament during the heat-up and melting phases of the plating operation. (4) Each source bead was assumed to be an isotropic point source of metal vapor, thereby ignoring both the effects of the wire passing through the bead and the finite size of the bead in computing the spatial distribution of the vapor flux from each source. (5) The residual gas pressure during plating was assumed to be small enough so that the effects of collision between metal vapor and residual gas might either be ignored or at least assumed constant over the different path lengths involved, specifically the distances from any fixed point on the substrate to each source bead on the filament. Plating pressures of 10^{-5} mm of mercury as employed in this work made such an assumption reasonable. (6) The accommodation coefficient was assumed to remain constant for all points on the substrate. Indeed, Langmuir (see Dushman (20)) has shown that the accommodation coefficient for systems of this type is very nearly unity.

Using these observations and assumptions, a plating model was formulated which was thought to simulate approximately the actual plating operation. For demonstration purposes two cases are presented in this chapter. The first case may be called the "ideal" plating operation, the second case the "typical" condition. The "ideal" condition was defined by a total of eight equally spaced sources with one source on each end of the filament. The "typical" condition was defined by a total of six sources with one source on each end of the filament, one source at the filament center, two of the remaining sources equally spaced between the filament center and one end, and the last source midway between the center and the opposite end. In addition, the source line (filament) was moved slightly off the substrate center line for the "typical" analysis. Figure 25 presents the source geometries for each case plus the coordinate nomenclature required for the plating model derivation.

Consider any source point, for example the nth point in a set of N total sources, and denote its strength as S_n (mass units/unit time). Denote its position by the point (x_n, y_n, h). The mass flux along the vector from the source (x_n, y_n, h) to any given substrate sample point (x_i, y_j, o) at the point (x_i, y_j, o) is given by:

$$\phi(x_i, y_j)_n = \frac{S_n}{4\pi r^2} \left(\frac{\text{mass units}}{\text{unit normal area - unit time}} \right) , \qquad (1)$$

where r is the length of the vector connecting (x_n, y_n, h) and (x_i, y_j, o). From Figure 25 it can be seen that r^2 in each specific case to be considered in this chapter is given by:

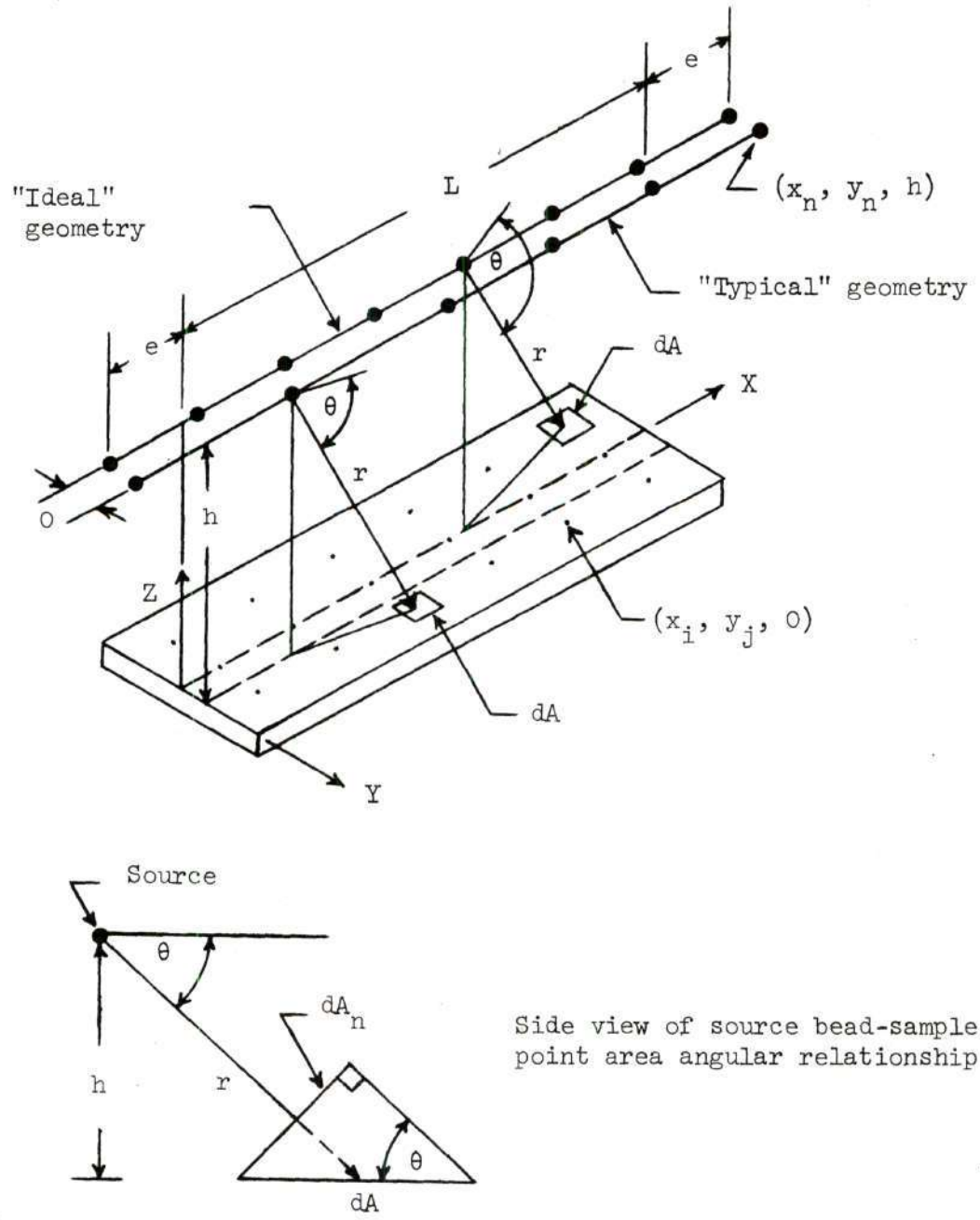

Side view of source bead-sample point area angular relationship

Figure 25. Source-Substrate Geometry and Nomenclature for Theoretical Thickness Distribution Calculation

$$r^2(\text{ideal}) = \left[h^2 + (x_i - x_n)^2 + y_j^2\right] \quad , \tag{2}$$

$$r^2(\text{typical}) = \left[h^2 + (x_i - x_n)^2 + (y_j - y_n)^2\right] . \tag{3}$$

Also from Figure 25, it can be seen that:

$$\frac{dA_n}{dA} = \cos\,(90^\circ - \theta) = \sin\theta = h/r \quad . \tag{4}$$

The mass flux in terms of a unit area in the xy plane can now be computed by:

$$M(x_i, y_j)_n = \phi(x_i, y_j)_n \left(\frac{dA_n}{dA}\right) = \phi(x_i, y_j)_n\,(h/r) \quad . \tag{5}$$

Thus, for the "ideal" case there is obtained

$$M(x_i, y_j)_n = \left(\frac{S_n}{4\pi}\right)\left(\frac{h}{\left[h^2 + (x_i - x_n)^2 + y_j^2\right]^{3/2}}\right) \quad , \tag{6}$$

and for the "typical" case,

$$M(x_i, y_j)_n = \left(\frac{S_n}{4\pi}\right)\left(\frac{h}{\left[h^2 + (x_i - x_n)^2 + (y_j - y_n)^2\right]^{3/2}}\right) \quad . \tag{7}$$

If t_p denotes the time of plating, and ρ the density of the plated metal, then the general expression for the thickness at the point (x_i, y_j) from all N sources would be:

$$\lambda(x_i, y_j) = \frac{1}{\rho} \sum_{n=1}^{N} \int_{o}^{t_p} M(x_i, y_j)_n \, dt \quad . \tag{8}$$

If $\bar{S}_n$ is defined as the total mass evaporated from the nth source point, there results

$$\bar{S}_n \equiv \int_{o}^{t_p} S_n \, dt \quad . \tag{9}$$

Since equal sources were assumed for this treatment, the thickness at the point (x_i, y_j) due to all N sources in the "ideal" case can now be calculated by:

$$\lambda(x_i, y_j) = \frac{\bar{S}_n}{4\pi\rho} \sum_{n=1}^{8} \frac{h}{\left[h^2 + (x_i - x_n)^2 + y_j^2\right]^{3/2}} \quad , \tag{10}$$

and for the "typical" case by:

$$\lambda(x_i, y_j) = \frac{\bar{S}_n}{4\pi\rho} \sum_{n=1}^{6} \frac{h}{\left[h^2 + (x_i - x_n)^2 + (y_j - y_n)^2\right]^{3/2}} \quad . \tag{11}$$

For manipulation purposes, equations (10) and (11) were rearranged as follows:

$$\lambda(x_i, y_j)\ \text{"ideal"} = \frac{\bar{S}_n}{4\pi\, h^2 \rho} \sum_{n=1}^{8} \frac{1}{\left[1 + \left(\frac{x_i - x_n}{h}\right)^2 + \left(\frac{y_j}{h}\right)^2\right]^{3/2}} \quad , \tag{12}$$

and

$$\lambda(x_i, y_j)\ \text{"typical"} = \frac{\bar{S}_n}{4\pi h^2 \rho} \sum_{n=1}^{6} \frac{1}{\left[1 + \left(\frac{x_i - x_n}{h}\right)^2 + \left(\frac{y_j - y_n}{h}\right)^2\right]^{3/2}} \quad (13)$$

From equations (12) and (13) it is obvious that the ratio of $\lambda(x_i, y_j)$ to the parameter $(\bar{S}_n/4\pi h^2\rho)$ might be considered a dimensionless thickness which is proportional to the actual thickness at each point. These ratios for both plating setups were computed for the eighteen points corresponding to the centers of the eighteen zones examined experimentally per substrate and plotted as the theoretical thickness distribution profiles in Figure 26. The numerical values of the ratios are listed in Table 20 of Appendix I.

The plating system dimensions used in these calculations were (see Figure 25): O = 0.125 inch, h = 1.5 inches, L = 3 inches, and e = 0.5 inch. The substrate sample point coordinates in parts of an inch were as follows:

	x_1	x_2	x_3	x_4	x_5	x_6
x	0.25	0.75	1.25	1.75	2.25	2.75
y_1	0.25	0.25	0.25	0.25	0.25	0.25
y_2	0.0	0.0	0.0	0.0	0.0	0.0
y_3	-0.25	-0.25	-0.25	-0.25	-0.25	-0.25

The source coordinates in parts of an inch for the "ideal" case were:

n	1	2	3	4	5	6	7	8
x	-0.5	0.072	0.644	1.216	1.788	2.360	2.930	3.50
y	0	0	0	0	0	0	0	0

"Ideal" Plating
Condition Profile

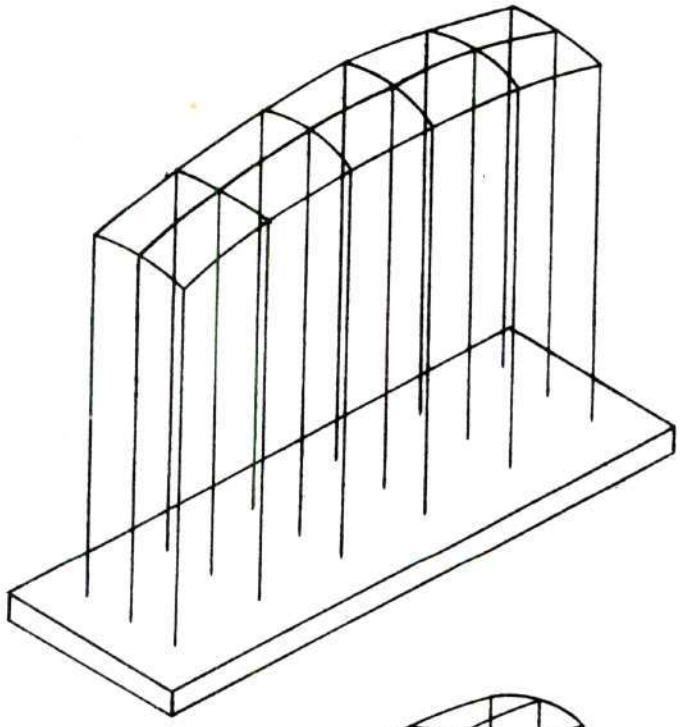

"Typical" Plating
Condition Profile

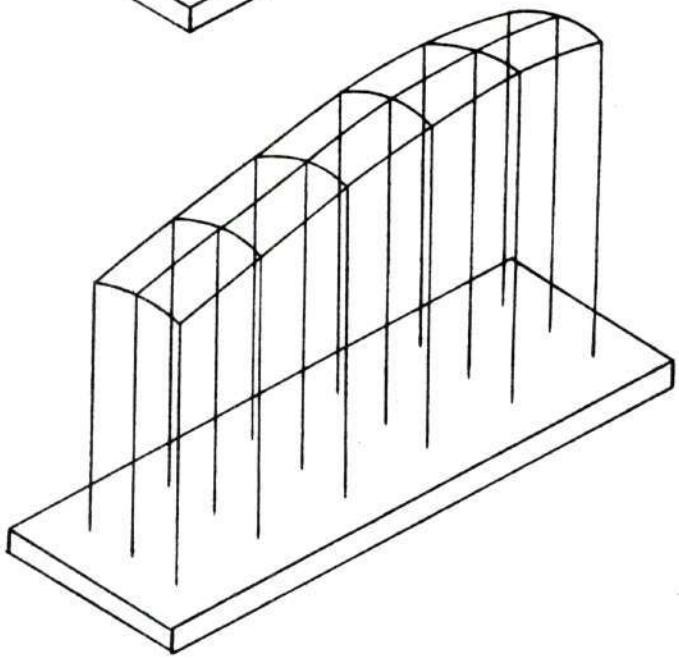

Figure 26. Theoretical Thickness Distribution Profiles for "Ideal" and "Typical" Plating Conditions

The source coordinates in parts of an inch for the "typical" case were:

n	1	2	3	4	5	6
x	-0.5	0.5	1.5	2.167	2.834	3.50
y	0.125	0.125	0.125	0.125	0.125	0.125

Discussion of Film Thickness Uniformity Results

Based on the results of the "ideal" analysis, film thickness distribution should be symmetrical about the substrate center. Along the longitudinal axis, the thickness at the substrate ends should be approximately 12 per cent less than that at the film center. The thickness of the off-axis points should be approximately 4 per cent less than that of the corresponding axial point. In terms of average thicknesses, the minimum thickness segments (at each end) would be expected to have a segment average thickness 7 per cent less than the overall average film thickness.

The results of the "typical" analysis indicated a skewed thickness distribution was likely for each film. In terms of segment average thicknesses, the minimum thickness segment (at one end) should have an average thickness approximately 24 per cent less than that of the maximum thickness segment (near the opposite end). Indeed, the minimum thickness segment would be expected to have a segment average thickness approximately 16 per cent less than the overall film average thickness. Cross axis variation was such that the minimum thickness in any segment would be expected to be approximately 6 per cent less than the maximum thickness in that segment.

Examination of the experimental data of Figures 21 through 24 and Tables 18 and 19 of Appendix I indicated that Copper Uniformity Films Nos. 1 and 2 behaved similarly to that predicted by the "typical" analysis, with

the only significant difference being in the "over-twisted" behavior observed in segment six of both films. Nickel Uniformity Films Nos.1 and 4 were also approximated by the "typical" analysis. Copper Uniformity Film No. 3 and Nickel Uniformity Film No. 2 were both closely approximated by the "ideal" analysis save for a few small local twists and dips. Indeed, the longitudinal axis variation of the segment average thickness for these two films appeared to be less than that predicted by the "ideal" analysis. Nickel Uniformity Film No. 3 is not approximated by either case presented and may, therefore, be thought of as being representative of the poorer quality nickel films produced for this work. Though not presented in this chapter, a distribution similar to that of Nickel Uniformity Film No. 3 is readily obtained from the plating model developed, assuming a source geometry of only a few effective source beads bunched near the ends of the source filament. Such a geometry, particularly in the case of nickel, was indeed observed to occur as related in the discussion of the plating difficulties presented below.

The major experimental difficulties encountered in this study were as follows: (1) For the thickness range of interest for each metal investigated the film weight deposited on each substrate sample segment approached the limiting sensitivity of the Mettler balance. Consequently, great care was required in sample preparation and handling in order to establish as uniform a procedure as possible for the weight data collection. Such techniques as frequent reweighing before and after plating were applied until successive weights were in satisfactory agreement. In addition, care was taken to insure that the sample was in thermal and adsorption equilibrium with the ambient environment before any weights were obtained.

(2) For the wire wrapped filament plating metals, copper and aluminum, great care was required in wrapping the filament to insure good thermal contact between the plating wire and the tungsten filament. In addition, it was found necessary to form the wrapped wire into a number of small coils, rather than one long continuous coil, and to secure the ends of each coil to the filament. If these techniques were not used, the plating wires would melt first at the points of good contact, break the continuous coil at these points, and cause the relatively long coils between these points to unwind from the filament. This unwinding was sometimes observed to throw molten metal from the ends of the coil. Should a thrown metal bead land on the substrate, the film had to be rejected for analysis. Even if the beads missed the substrate, however, the film quality was reduced due to the fewer number of available source beads on the filament and their less uniform spacial distribution. Consistent use of the proper procedures, however, made the plating of copper and aluminum films simple from the manipulative point of view, and produced films of good thickness uniformity.
(3) In the case of nickel, the alloying of the molten nickel and the tungsten filament caused great difficulty in developing a suitable plating procedure. Nickel wire was first tried in a technique similar to that used for copper and aluminum. It was found, however, that as the nickel wire melted and beaded on the filament, alloying would occur more rapidly than the molten metal could be evaporated from the beads. The situation was compounded by the tendency to throw molten metal off the beads if the filament temperature were raised too rapidly. Consequently, each bead zone would progressively become a region of high resistance and increasing brittleness. Quite frequently, filament breakage would occur at the end beads well before suffi-

cient nickel had been deposited on the substrate. In an effort to increase the number and reduce the size of the beads, it was decided to attempt the use of a filament which had been electroplated with a thin sheath of pure nickel. This technique, with careful control and much practice, did permit the satisfactory plating of nickel films for this work. However, film rejection due to filament breakage continued to be a major problem, and invariably in successful platings one or more beads could not be completely plated due to alloying and imminent filament breakage. Such incomplete evaporation would, of course, reduce the nickel uniformity and therefore account for the generally less uniform nature of the nickel films observed in the experimental results of this chapter as well as the poorer agreement between the experimental data and the theoretical analysis for nickel. (4) The remaining experimental problem of X-ray source intensity drift has already been discussed earlier in this chapter.

In view of the problems encountered, the good agreement obtained between theory and experiment in this study provided a foundation for the quantitative interpretation of these data in the modeling of film thermal behavior presented in Chapter VI. Although it would have been desirable to apply the X-ray technique to each heat transfer film prior to its thermal test and to use the calibration curves to compute its thickness distribution, the limited size of the X-ray sample holder, the possibility of damaging the film surface during the positioning of the sample in the holder, and the unknown effects that X-ray ionization damage to the film matrix might have on the thermal behavior of the film precluded such an operation. However, because of the special care taken to plate the segmented substrates in this study in an identical manner with the thermal

test samples, the results of this study are thought to be typical of and applicable to the thermal test films.

CHAPTER VI

RESULTS AND DISCUSSION OF THE VACUUM THERMAL TESTS

The equipment and experimental techniques designed to facilitate the investigation of the intrinsic thermal behavior and limitations of thin metal films have been presented in detail in Chapters II and III. This was done to provide a background into the limitations of the thermal measurements now presented, and because a sizeable portion of the research program had to be devoted to technique coordination and mastery. Chapters IV and V presented summaries of measured film properties and characteristics both for completeness and for interpretation of the thermal test results.

This chapter will first present the results of the vacuum thermal tests for each film metal. Then, utilizing an analytical model for the substrate conduction in combination with the measured film temperature history, a comparison between the measured film heat flux and the computed heat flux based upon the measured film temperature will be performed. This comparison was made to provide an independent check on the film calibration procedures, the recording system calibration techniques, and the photographic withdrawal and data reduction. In short, the comparison served to verify the validity of the entire experimental procedure as well as to aid in the film failure analysis.

The thickness distribution data of Chapter V were quantified, combined with the appropriate experimentally measured film parameters, and

used to formulate several "notch" models of internal film behavior at or near the measured failure point for each test run. These modeling analyses attempted to estimate the temperature in the thin and thick regions of the film in order to correlate better the local film conditions with the measured film average properties at failure. Coupling of the measured thermal test film data and the "notch" analyses results with visual observations of the test film behavior and response provided considerable insight into thin film failure mechanisms and their intrinsic limitations as thermometric transient heating surfaces. Of course, the externally heated film data of Chapter IV provided a base line for much of the transient data interpretation presented in this chapter.

Thin Film Thermal Test Data

Complete data for each vacuum thermal test film are tabulated in Appendix II and plotted in Appendix III. Figures 27 through 29 present summary plots of film temperature versus film heat flux, i.e., input power per unit film surface area for copper. Figures 30, 31, 32, and 33 present similar data for nickel and aluminum films, respectively. The data in these figures are grouped according to film test time with the exception of Figure 33, which contains a summary of the aluminum film data incompletely recorded due to saturation of the voltage channel recording oscillator (see the discussion in Chapter II relative to underattenuation of the voltage signal). Table 3 summarizes the measured film failure conditions. Figures 34 through 36 present photographs of the post-test copper films grouped in accordance with the data of Figures 27 through 29. Figures 37 and 38 present the nickel post-test films grouped in accordance with the data of